aerospace

MDPI

Article

A Physics-Based Multidisciplinary Approach for the Preliminary Design and Performance Analysis of a Medium Range Aircraft with Box-Wing Architecture

Karim Abu Salem [1,*], Vittorio Cipolla [1], Giuseppe Palaia [1], Vincenzo Binante [2] and Davide Zanetti [2]

[1] Department of Civil and Industrial Engineering, University of Pisa, Via G. Caruso 8, 56122 Pisa, Italy; vittorio.cipolla@unipi.it (V.C.); giuseppe.palaia@phd.unipi.it (G.P.)
[2] SkyBox Engineering, Via G. Caruso 8, 56122 Pisa, Italy; v.binante@skyboxeng.com (V.B.); d.zanetti@skyboxeng.com (D.Z.)
* Correspondence: karim.abusalem@ing.unipi.it

Abstract: The introduction of disruptive innovations in the transport aviation sector is becoming increasingly necessary. This is because there are many very demanding challenges that the transport aviation system will have to face in the years ahead. In particular, the reduction in pollutant emissions from air transport, and its impact on climate change, clearly must be addressed; moreover, sustainable solutions must be found to meet the constantly increasing demand for air traffic, and to reduce the problem of airport saturation at the same time. These three objectives seem to be in strong contrast with each other; in this paper, the introduction of a disruptive airframe configuration, called PrandtlPlane and based on a box-wing lifting system, is proposed as a solution to face these three challenges. This configuration is a more aerodynamically efficient alternative candidate to conventional aircraft, introducing benefits in terms of fuel consumption and providing the possibility to increase the payload without enlarging the overall aircraft wingspan. The development and analysis of this configuration, applied to a short-to-medium range transport aircraft, is carried out through a multi-fidelity physics-based approach. In particular, following an extensive design activity, the aerodynamic performance in different operating conditions is investigated in detail, the structural behaviour of the lifting system is assessed, and the operating missions of the aircraft are simulated. The same analysis methodologies are used to evaluate the performance of a benchmark aircraft with conventional architecture, with the aim of making direct comparisons with the box-wing aircraft and quantifying the performance differences between the two configurations. Namely, the CeRAS CSR-01, an open-access virtual representation of an A320-like aircraft, is selected as the conventional benchmark. Following such a comparative approach, the paper provides an assessment of the potential benefits of box-wing aircraft in terms of fuel consumption reduction and increase in payload capability. In particular, an increase in payload capability of 66% and a reduction in block fuel per pax km up to 22% is achieved for the PrandtlPlane with respect to the conventional benchmark, while maintaining the same maximum wingspan.

Keywords: box-wing; PrandtlPlane; disruptive aircraft; innovation; future aviation

Citation: Abu Salem, K.; Cipolla, V.; Palaia, G.; Binante, V.; Zanetti, D. A Physics-Based Multidisciplinary Approach for the Preliminary Design and Performance Analysis of a Medium Range Aircraft with Box-Wing Architecture. *Aerospace* **2021**, *8*, 292. https://doi.org/10.3390/aerospace8100292

Academic Editor: Dieter Scholz

Received: 19 July 2021
Accepted: 29 September 2021
Published: 9 October 2021

1. Introduction

In the near future, the aviation industry will have to face several challenging tasks; the most relevant issue is related to the environmental impact of transport aviation, which has to drastically reduce its pollutant footprint and its impact on climate change [1–6]. At the same time, the demand for commercial air transport is growing quickly [7–10], whereas airports are gradually addressing saturation problems using aprons [11]. Meeting the growing demand for flights and reducing the environmental impact of air transportation seem to be contrasting objectives of aviation research and industry; a possible way to face this problem is to explore and study disruptive technologies, both in the field of propulsion

and aircraft design. Regarding propulsion, several studies are dedicated to the analysis and design of new types of engines, alternative to the conventional internal combustion one, such as hybrid and electrical powertrains [12–17]; also, alternative energy sources to fossil fuels, such as hydrogen [18–21] or biofuels [22–24], are currently under study. Regarding aircraft development, studies have been conducted on the optimisation of the tube-and-wing aircraft to reach the maximum potential of the conventional configuration [25–28], but great effort is currently dedicated to the study and development of new unconventional architectures [29–34], such as the blended wing–body configuration [35–37] or the joined wings architecture [38,39], which may represent a real breakthrough in aircraft evolution.

In this paper, the focus is on an unconventional configuration called PrandtlPlane [40–43], a concept based on the box-wing lifting architecture, which is represented in Figure 1; for the PrandtlPlane (PrP) configuration, the box-wing is designed according to Prandtl's "best wing system" theory [44], which allows one to minimise the induced drag of the lifting system [45,46]. This configuration has been extensively studied in the PARSIFAL project [47,48], a research project funded by the European Commission in the framework of the Horizon2020 program.

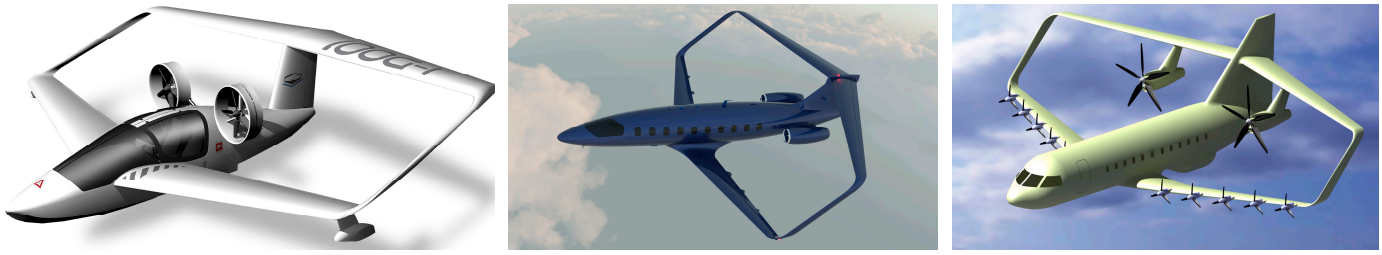

Figure 1. Artistic views of PrandtlPlane aircraft of different categories: ultra-light amphibious (**left**) [43], executive class (**centre**) [49], hybrid electric regional airliner (**right**) [15].

Some of the main challenges that will be faced by aeronautical research in the near future are summarised in Table 1, together with some general possible solutions.

Table 1. Challenges ahead for the transport aviation and related general solutions.

Challenge	Possible Solution
To meet the large air traffic demand increase expected in the coming years, in particularly for short/medium routes [7] *.	To design an aircraft with an increased cabin capacity compared to the present aircraft operating on short/medium routes.
To avoid airport saturation problems, already relevant today [11].	To limit the size and overall dimensions of the aircraft.
To reduce the environmental impact of the aircraft [2], thus minimising fuel consumption per passenger.	To increase the aerodynamic efficiency as much as possible and/or to adopt new types of propulsion (i.e., electric or hydrogen).

* The forecasts used as reference were provided before the COVID-19 outbreak; the pandemic will have a direct impact on the air traffic demand and on the related forecast. The main consequence is related to a shift-forward of the peak increase in the demand with respect the previous market outlooks. However, the overall scenario is supposed to be the same, in a delayed time scale.

To effectively address the issues ahead, aircraft configuration must comply with the three indicated solutions at the same time. Concerning the issue of the saturation of airport areas, it should be pointed out that using larger existing aircraft to reduce the number of flights does not represent a solution to the problem; for example, using an Airbus A350 in place of two Airbus A321s on medium-haul flights (leaving aside the fact that A350 aircraft are not designed to accomplish these missions) would reduce the number of slots occupied, but the size of the Airbus A350 would require the occupation of a much larger apron (ICAO Aerodrome Code C: max wingspan 36 metres vs. ICAO Aerodrome Code E: max wingspan 65 m) and taxiway. It is clear that this operation does not bring any advantages. On the contrary, it would imply further disadvantages, considering the fact that the majority of

worldwide airport slots are represented by ICAO C aprons, while there are significantly fewer ICAO E aprons [50].Wingspan definitely plays a key role in ground operations, as it is constrained by the standardised dimensions of the apron and taxiways.

The general solutions proposed to the three challenges presented above indicate that a technological step forward is necessary for commercial aviation aircraft: it is difficult to try to solve these problems through the adoption of aircraft with conventional architecture and/or conventional propulsion system [51].

In this work, a suitable solution to the presented challenges is proposed through the introduction of the non-conventional PrandtlPlane architecture, while aspects related to innovative propulsion systems are not considered; in particular, a detailed analysis is conducted to answer the question: "can the introduction of the PrandtlPlane configuration be a possible solution to face the challenges of commercial aviation in the near future?"

The PrandtlPlane configuration is a candidate to satisfy the three challenges previously presented; in particular, considering the short/medium-haul market sector, it allows:

1. The transport of a larger number of passengers compared to the present aircraft operating on medium routes, by exploiting the increased lifting capacity of the box-wing system, and using a new fuselage design, in order to increase the number of travellers without increasing the number of flights;
2. The exploitation of the increased lifting capacity of the box-wing to design an aircraft with the same overall dimensions, in particular of wingspan, of present aircraft operating on short/medium routes, while improving the passenger capability, in order to avoid the increase in required apron space; namely, this requires the design of a box-wing with wingspan limited to the standard related to short-to-medium-route aircraft, i.e., maximum 36 m (ICAO Aerodrome Code C), to be compliant with the airport infrastructure (aprons, taxiways), but at the same time, to transport a larger payload;
3. The exploitation of the box-wing architecture designed according to the "Best Wing System" theory to maximise the aerodynamic efficiency; indeed, a properly designed box-wing aircraft allows one to theoretically minimise the induced drag, by exhibiting Oswald factor efficiencies larger than 1 [45], as well as to increase the lifting capability (i.e., to trim a larger weight), and thus to reduce the fuel consumption per passenger–kilometre compared to conventional aircraft.

In this paper, first of all, the multidisciplinary design methodology adopted to develop a short/medium-haul PrandtlPlane aircraft is presented by describing the multi-fidelity design and analysis strategy implemented in detail. The main focus is given to the aerodynamic and structural design of the innovative box-wing lifting system, together with a detailed assessment of the mission performance. Then, the PARSIFAL project case study is presented and described in detail, starting from the definition of the design requirements to the aerodynamic and mission performance evaluation. The box-wing aircraft performance are then compared with those of a reference conventional tube-and-wing benchmark aircraft; the performance assessment methods used are the same in both cases, to provide direct and fair comparisons between two totally different aircraft architectures.

2. Design Methodology Description

The design strategy adopted for the development of the box-wing aircraft is schematically summarised in Figure 2; three main different stages were performed: a conceptual design initialisation, a reference aerodynamic layout definition through aerodynamic optimisation and a subsequent model refinement and performance evaluation. These three main blocks of the design process are detailed in the following.

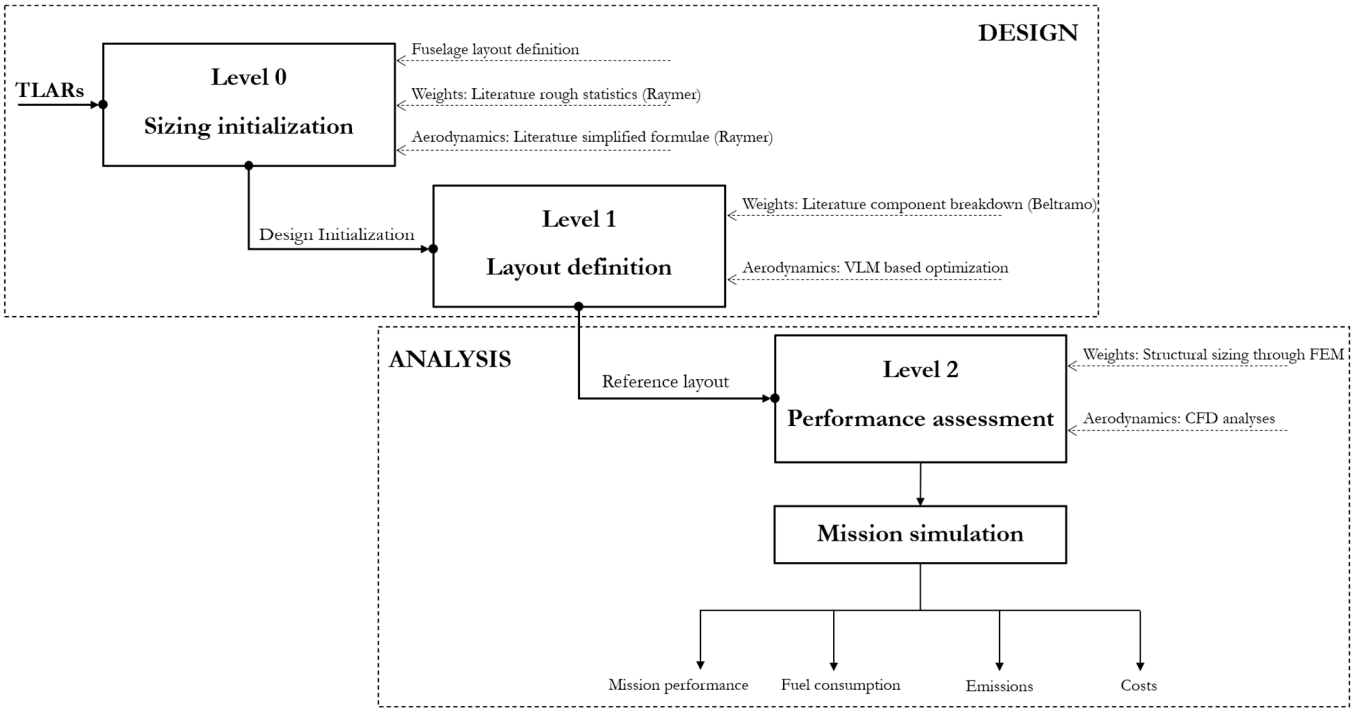

Figure 2. Multi-level aircraft design and analysis diagram (abbreviations used: VLM = Vortex Lattice Method, FEM = Finite Element Model, CFD = Computational Fluid Dynamics).

2.1. Conceptual Design Initialisation

The first step of the initial conceptual sizing is represented by the definition of the fuselage layout, its overall size, and the characterisation of the cabin section layout and the internal arrangement; this is fundamental, because one of the main requirements to be satisfied is represented by the maximum number of passengers: to accomplish this specification, a proper fuselage design is needed to start the following aircraft design process. Then, the conceptual design initialisation mainly consists of a rough evaluation of the aircraft aerodynamic performance and the related estimation of the initial guess of the maximum take-off weight. The inputs of the procedure are the Top Level Aircraft Requirements (TLARs), namely the design payload and range, the operating conditions and the size constraints. As far as the aerodynamic performance is considered, a simplified model to estimate the aircraft drag was used by separately calculating the induced drag coefficient, C_{Di}, the parasite drag coefficient, C_{D0}, and the wave drag coefficient, C_{Dwave}, of the aircraft (Equation (1)).

$$C_{D\ tot} = C_{Di} + C_{D0} + C_{D\ wave} \tag{1}$$

The induced drag coefficient, C_{Di} , is estimated by considering only the lifting components (Equation (2)); namely, the contribution of the front and rear wings are considered, as the contributions to the induced drag of the vertical wings and the fuselage are neglected at this stage.

$$C_{Di} = C_{Di}^{Front} + C_{Di}^{Rear} + \cancel{C_{Di}^{Vertical}} + \cancel{C_{Di}^{Fus}} \tag{2}$$

The induced drag coefficient, C_{Di}^{wing} , of each lifting component is evaluated by using the relations of Equations (3)–(4), where C_L represents the wing lift coefficient, AR is the related aspect ratio, and e is the Oswald factor. As the considered configuration is a box-wing designed according to the Prandtl's theory on the best wing system [44], the Oswald factor, e, used in this phase is fixed equal to 1.46 [52]. Since the aircraft geometry does not exist at this initialisation stage, some reference parameters must be set reasonably, as indicated in the reference literature. This is the case for the Oswald factor, as, although it

depends on the wings' height to span ratio, h/b [44], it is set as equal to the theoretical maximum value for a box lifting system [52]. This does not represent a misalignment, since in the following design phases (Section 2.2) the Oswald factor is calculated for each configuration considered (taking into account its geometrical and lift distribution characteristics) by means of the VLM aerodynamic solver.

$$C_{Di}{}^{wing} = kC_L{}^2 \tag{3}$$

$$k = 1/(\pi\, AR\, e) \tag{4}$$

The parasite drag coefficient, C_{D0}, is evaluated by the *equivalent skin friction model* described in [53]; namely, the $C_{D0\ tot}$ of the aircraft is the sum of each aircraft component, $C_{D0}{}^{comp}$, evaluated by means of the formula of Equation (5).

$$C_{D0}{}^{comp} = C_{fe}\ (S_{wet}{}^{comp}/S_{ref}) \tag{5}$$

$$C_{D0\ tot} = \Sigma C_{D0}{}^{comp} \tag{6}$$

where C_{fe} is the equivalent skin friction coefficient, equal to 0.0030 for civil transport aircraft from the approximation reported in [53]; the same reference presents a simplified way to estimate the components' wetted surface, $S_{wet}{}^{comp}$, both in the case of a wing component (i.e., lifting surfaces, vertical tip-wing, tail, fin, Equation (7)) and cylindrical components (i.e., fuselage, nacelle, Equation (8)):

$$S_{wet}{}^{Wing} = S_{exposed}\ [1.997 + 0.52\ (t/c)] \tag{7}$$

$$S_{wet}{}^{cyl} = \pi\, d^{cyl} l^{\,cyl} \tag{8}$$

where $S_{exposed}$ is the planform area of the wing exposed to the flow, (t/c) is the wing thickness-to-chord ratio, and d^{cyl} and l^{cyl} are the diameter and the length, respectively, of the considered cylinder. For aircraft cruising in transonic flight, the wave drag coefficient, C_{Dwave}, is fixed as constant and equal to 0.002, according to the Boeing definition of transonic drag rise reported in [53].

Several simplified models are presented in the literature to evaluate the aircraft gross weight in the very initial stage of the aircraft design. In this phase, to initialise the design process, the aircraft maximum take-off weight, *MTOW*, is estimated by individually evaluating the contribution of the payload weight, W_{pay}, the fuel weight, W_{fuel}, and the operating empty weight, W_{oe} (Equation (9)):

$$MTOW = W_{pay} + W_{fuel} + W_{oe} \tag{9}$$

where, concerning the payload, 95 kg per passenger is assumed ([54]), the fuel weight, W_{fuel}, is evaluated by using the well-known Breguet formula [55], and the operating empty weight, W_{oe}, is estimated by the statistic interpolation of historical trends proposed in [53].

2.2. Optimisation Driven Preliminary Design

The main information obtained from the conceptual design initialisation is the first estimation of the aircraft maximum take-off weight, which is useful to start the second level of the aircraft design process (Figure 2). In particular, in this stage, the aerodynamic design is driven by an optimisation procedure implemented in an in-house tool called AEROSTATE [56–58]; the schematic representation of the AEROSTATE code is reported in Figure 3.

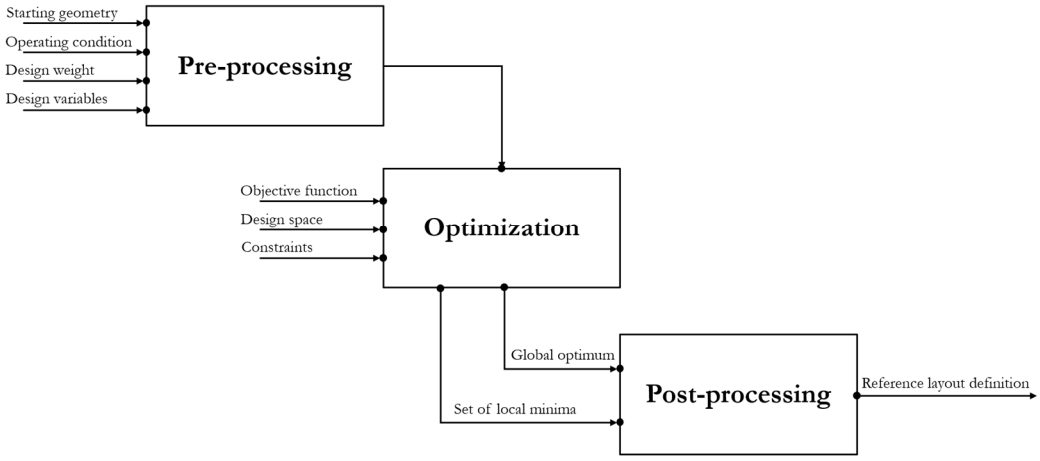

Figure 3. AEROSTATE workflow.

The general constrained aerodynamic optimisation problem addressed in this tool is summarised in the following Equations (10)–(12):

- Objective function

$$\min(-L(\boldsymbol{x})/D(\boldsymbol{x})) \tag{10}$$

- Set of inequality constraints

$$g(\boldsymbol{x}) \geq 0 \tag{11}$$

- Design space

$$\boldsymbol{lb} < \boldsymbol{x} < \boldsymbol{ub} \tag{12}$$

where the objective function to be minimised is the -*L*/*D* ratio, which is equivalent to the maximisation of the aerodynamic efficiency (lift-to-drag ratio) evaluated in a reference point of the cruise (e.g., the 25% of the stage length); the optimisation is constrained by a set of inequality constraints $g(\boldsymbol{x})$; the design variables $\boldsymbol{x}$, limited by lower and upper boundaries ($\boldsymbol{lb}$ and $\boldsymbol{ub}$, respectively), are reported in Figure 4.

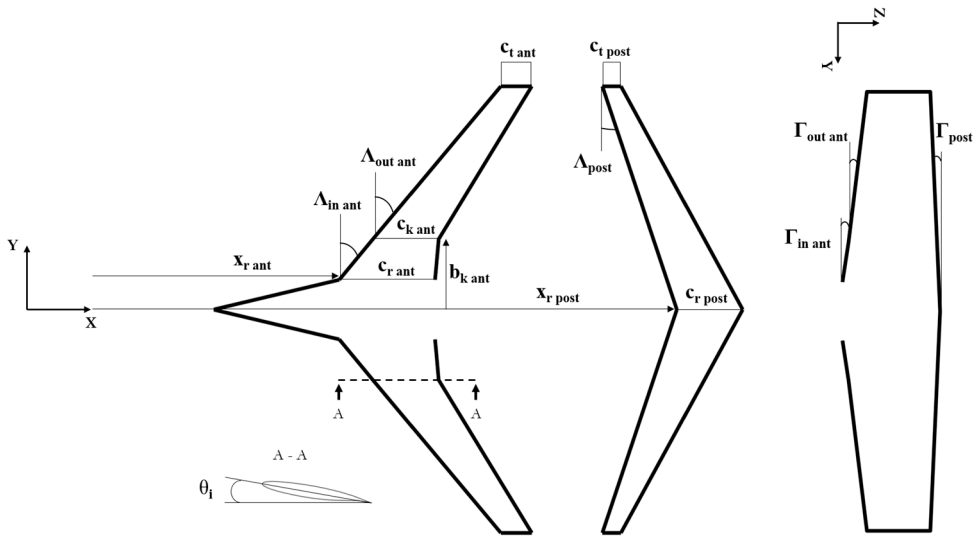

Figure 4. Design variables of the aerodynamic optimisation.

The optimisation tool allows one to introduce constraints to search feasible configurations, from aerodynamic and aeromechanic standpoints; the set of inequality constraints are summarised in Equations (13)–(19):

- Vertical trim

$$W_{des} - \varepsilon_L \leq L(\boldsymbol{x}) \leq W_{des} + \varepsilon_L \tag{13}$$

- Longitudinal static stability

$$SSM_{\min} \leq SSM(\boldsymbol{x}) \leq SSM_{\max} \tag{14}$$

- Pitch trim

$$-\varepsilon_M \leq C_M(\boldsymbol{x}) \leq \varepsilon_M \tag{15}$$

- Max local lift coefficient

$$\max(c_l(y, \boldsymbol{x})) \leq \hat{c}_{lTH} \tag{16}$$

- Wing loading constraints

$$(L/S)_{\min} \leq (L(\boldsymbol{x})_{wing}/S(\boldsymbol{x})_{wing}) \leq (L/S)_{\max} \tag{17}$$

- Taper ratio

$$\lambda_j(\boldsymbol{x}) < 1 \tag{18}$$

- Relative wings position

$$x_{LE\ tip}^{front\ wing} + c_{tip}^{front\ wing} < x_{LE\ tip}^{rear\ wing} + \Delta x \tag{19}$$

where W_{des} is the input design weight; SSM is the longitudinal static stability margin; C_M is the pitching moment coefficient; $c_l(y)$ is the spanwise distribution of local lift coefficient and $\hat{c}_{lTH}$ is the related threshold value; $\left(L_{wing}/S_{wing}\right)$ is the *i-th* lifting surface wing loading; λ_j is the *j*-th wing bay taper ratio; $x_{LE\ tip}$ is the longitudinal position of the wing tip leading edge; c_{tip} is the wing tip chord; ε is a tolerance. Several details about the optimisation procedure and algorithms implemented in the AEROSTATE tool are described in [58–60]. This tool evaluates the lift-to-drag ratio at the reference design point by estimating the overall drag, as reported in Equation (1); nevertheless, in this case, the geometry of the lifting system is known, as it is computed at each iteration of the optimisation process, so the parasite drag coefficient of the wing components, ${C_{D0}}^{Wing}$ (i.e., front/rear wing, vertical tip-wing, fin), is computed by integrating spanwise the airfoil drag contribution, as expressed in Equation (20):

$${C_{D0}}^{Wing} = \frac{1}{S_{ref}} \int_{-b}^{b} C_{D\ foil}(y)\ c(y)\ dy \tag{20}$$

where the function $C_{Dfoil} = f(Re, M, C_{Lfoil})$ is calculated by Xfoil [61] and is provided as input to the procedure, S_{ref} is the wing reference surface, and $c(y)$ is the spanwise chord distribution. The ${C_{D0}}^{Fus}$ is computed by means of the *component build-up method* described in [53]; in particular:

$${C_{D0}}^{Fus} = Q\ C_f\ FF\ \frac{S_{fus}}{S_{ref}} \tag{21}$$

where the friction coefficient, C_f, the form factor, FF, and the interference factor, Q, are reported in [53]. Concerning the lift induced drag, once the design weight is defined as

an input, the optimiser uses a Vortex Lattice Solver to evaluate the vertical trim condition (Equation (13)), and so extracting the aircraft $C_{L\,trim}$ and C_{Di} values. The solver used is the Vortex-Lattice-based AVL [62], and a typical representation of a box-wing configuration within this solver is reported in Figure 5.

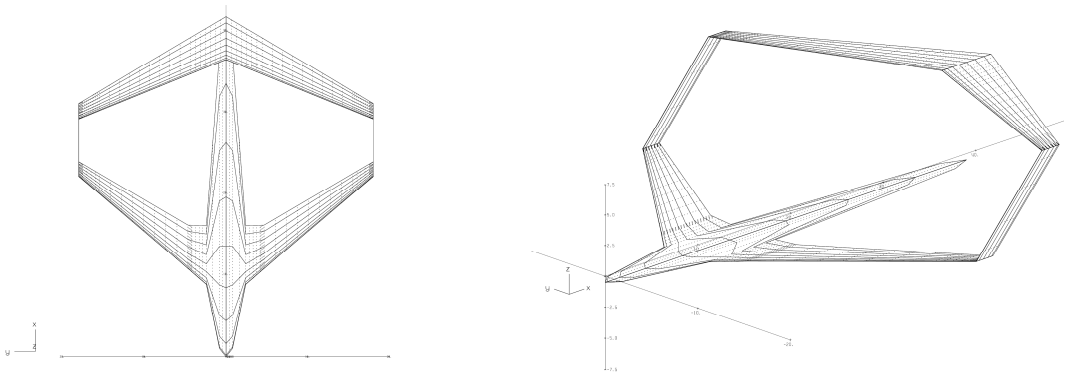

Figure 5. AVL model for a box-wing configuration.

As it is chosen to represent the fuselage as a flat plate in AVL, the vertical trim is evaluated in AVL with the fuselage always aligned to the flow; namely, the trim is solved with the angle of attack $\alpha = 0°$, and by acting on the wings' twist distributions, so as to not introduce the lift-induced drag coming from the simplified fuselage modelling.

Additionally, in this second block of the design process, the maximum take-off weight of the aircraft is evaluated by means of the breakdown described by Equation (9); again, the payload and the fuel weight are calculated as described in Section 2.1, while the operating empty weight is subdivided as follows:

$$W_{oe} = W^{Wings} + W^{Fus} + W^{Eng} + W^{Sys} + W^{Oper} \tag{22}$$

where W^{Wings} represents the weight of the lifting system, W^{Fus} is the fuselage weight, W^{Eng} is the engine weight, W^{Sys} represents the weight of the on-board systems, and W^{Oper} represents the weight of the aircraft operating items. As the geometry of each configuration designed in this phase is known, single contributions can be estimated by means of slightly more accurate methods than those used in the initialisation phase; in particular, the wing weight and the systems and operating weights are estimated by means of the method proposed in [63], and the fuselage weight and the engine weight are evaluated by means of the methodology used in [64]. During the optimisation, these estimations are also useful to evaluate the centre of gravity position, and so to evaluate the constraints concerning the pitch trim and the longitudinal stability.

At the end of the process, it is possible to select an aerodynamic layout provided in output from the optimisation process, and to re-estimate the maximum take-off weight by means of Equations (9) and (22); if this value differs from the input provided by the starting initialisation within a prescribed tolerance, the procedure is iterated until the convergence is reached (Figure 6).

Transonic Aerodynamic Assessment: Level 1 and 1/2

If the design process involves transonic aircraft, such as commercial medium/long range airliners, it is necessary to provide some information about the transonic behaviour of the lifting system from the conceptual stage of the design. This aspect is relevant as, after a specific condition in transonic flight called *drag rise*, the aircraft performance deteriorates severely; in particular, for certain combinations of cruise Mach number, trim lift coefficient and wings geometry, a massive drag increase occurs; this is caused by the rise in shock waves (wave drag contribution), and by the interaction of these waves with the boundary layer, that thickens until local separation is reached, causing increases in pressure drag.

The *drag rise* condition needs to be avoided in the whole standard operating envelope of an aircraft. However, the transonic phenomena are very difficult to be detected and properly described by the low-fidelity methods that are typically used in the conceptual stages of the design process to provide fast and adequately reliable assessments. This because the transonic phenomena strictly depend on the local geometry of the wings, on the airfoil shape, on the joints and on the fillets' design; moreover, transonic fluid physics is strongly three-dimensional and exhibits strong coupling and interaction between the boundary layer and the sonic phenomena such as shock waves. It is evident that potential methods, such as the VLM, cannot predict any of these physic phenomena, as they are not designed to take the fluid compressibility (and so the shock waves) and the fluid friction actions (and so the boundary layer) into account. In the literature, some simplified methods are provided that take transonic effect into account in the early stages of the design process: in [65], a quasi-3D model is presented, which couples a VLM solver with a strip model considering 2D airfoil transonic performance computed by means of a CFD solver; in [66], the wave drag coefficient is estimated by means of semi-empiric formulae provided by the Korn–Locke method. Although these methods are useful to identify relevant correlations between the aerodynamic performance and some macro-parameters (such as the airfoil shape, the wings' sweep angles, the thickness distribution and the local lift coefficient), they may fail to provide reliable absolute performance prediction to be used with enough confidence in the conceptual design phase. In other words, with these models, we cannot ensure that a specific design coming from the *Level 1* stage of the design process (Figure 2) is far from the *drag rise* conditions; this may compromise the development of the design, as it is possible to specifically evaluate the transonic performance only at *Level 2* stage of the design process (Figure 2), where higher fidelity methods as CFD RANS solver are used. To avoid that, the design of configurations at *Level 1* may present possible transonic issues at *Level 2*, and so to prevent restarting the design process from the beginning, a preliminary transonic assessment was performed for the specific design problem described in Section 3. In particular, a CFD campaign was carried out to improve the knowledge on the transonic behaviour of the box-wing lifting system, and to obtain information and data to calibrate the *Level* 1 aerodynamic optimisation set-up (design variables boundaries, aerodynamic constraints), with the aim of designing configurations that are confidently far from the *drag rise* condition; as this high-fidelity assessment was useful in properly tuning the *Level 1* design stage, this procedure can be used as a *Level 1 and* 1/2 block, parallel to the *Level 1* design block.

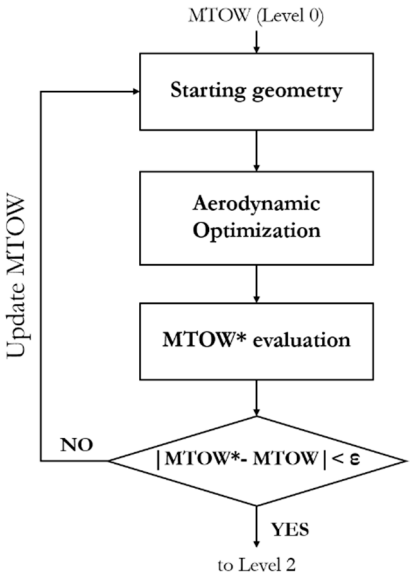

Figure 6. *Level 1* sizing procedure scheme.

Steady compressible RANS simulations were used to investigate the box-wing in transonic flight, and the performance correlation with some relevant parameters; in particular, a focus on some macro parameters together with an analysis on some local effects have been provided, as described in [67]. The airfoil that was selected to be used for the box-wing is a supercritical profile and it is not considered as a design variable. Concerning the macro parameters, major effort was given to the role of the wing loading (Figure 7) and to the wings' sweep angles; the effect of cruise Mach was investigated as well.

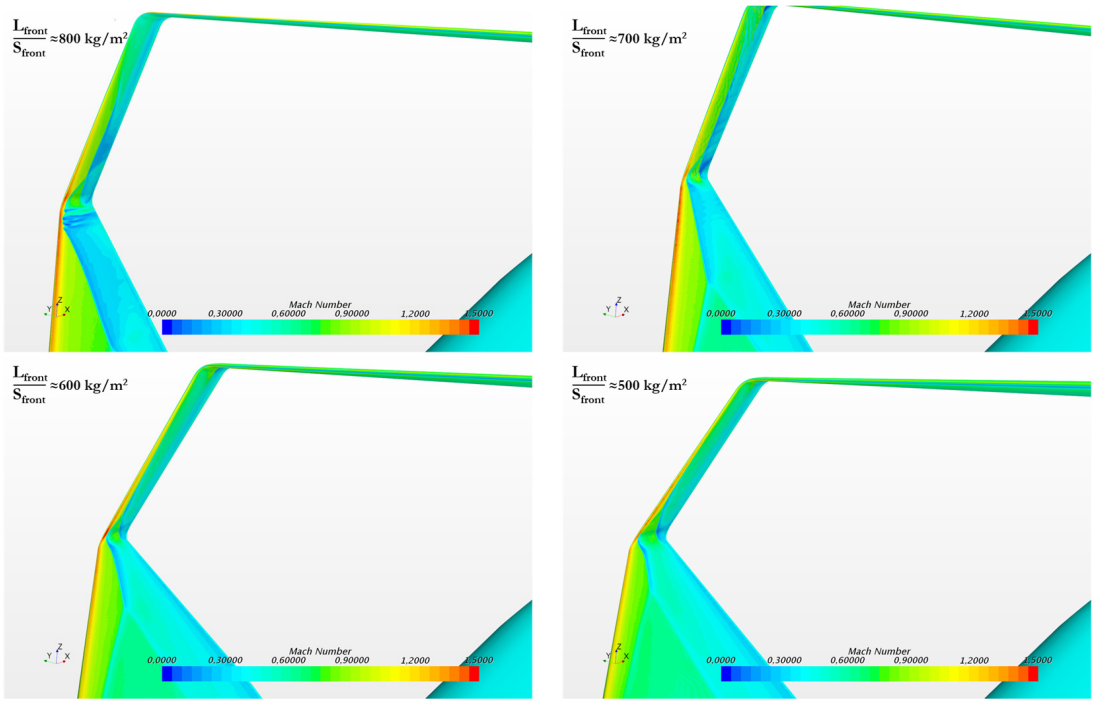

Figure 7. Wing loading variation effect on flow over the front wing (Mach contours @M_∞ = 0.79).

Some local geometrical parameters were identified as more influential with respect to the transonic drag increase; in particular, the twist distribution in the tip zone of the front wing proved to be crucial to be properly set in order to avoid detrimental shock-induced drag increase (Figure 8 (left)). The load of the front wing tip region is enhanced by the aerodynamic behaviour of a positive swept wing; moreover, differently from a conventional wing in which the tip is free, for the box-wing, there are flow accelerations on the fillet with the vertical wing, which ease the flow to reach sonic conditions. The opposite happens for the rear wing, as the aerodynamic behaviour of the forward swept wing leads to a spanwise enhancement of the lift coefficient in the root zone; moreover, in the root zone, there is a significant straightening of the isobars, as the rear wing is not directly constrained to the fuselage: this effect reduces the aerodynamic sweep of this portion of wing. These two features of the forward swept wing can lead to transonic issues in the root zone (Figure 8 (left)).

This qualitative information was then used to properly tune the *Level 1* optimisation framework for the preliminary aerodynamic design. A conservative design approach was chosen for this stage; in particular, a set of constraints and boundaries for the design variables was identified to allow the optimiser to design configurations that are confidently far from the detrimental transonic drag increase effects. For the design case described in Section 3, concerning a medium range transport box-wing aircraft, the boundaries/constraints selected are summarised in Table 2.

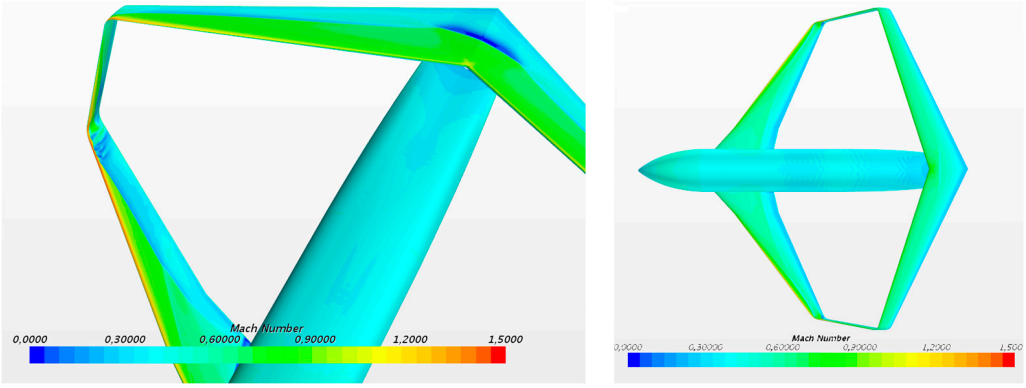

Figure 8. Local transonic critical issues (**left**); box-wing without transonic issues (**right**). Mach contours referring to freestream $M_\infty = 0.79$.

Table 2. *Level 1 and* 1/2 calibration of the preliminary aerodynamic optimisation.

Front wing loading, L_{front}/S_{front}	<600 kg/m^2
Rear wing loading, L_{rear}/S_{rear}	<600 kg/m^2
Front wing sweep angle, Λ_{front}	>35°
Rear wing sweep angle, Λ_{rear}	*free*
Cruise Mach	<0.79
Front wing tip twist angle, $\theta_{front}{}^{tip}$	<−1°
Rear wing root twist angle, $\theta_{rear}{}^{root}$	<+1°
Spanwise local lift coefficient, $c_l(y)$	<0.7

2.3. High-Fidelity Performance Assessment

2.3.1. Aerodynamic Performance

In the third phase (*Level 2*, Figure 2), the aerodynamic layout provided by the optimisation process was subject to refined analysis, concerning aerodynamics, structural sizing, weight estimation and performance assessment. First of all, the information gained through the design process allowed one to generate the 3D CAD model of the box-wing aircraft (Figure 9).

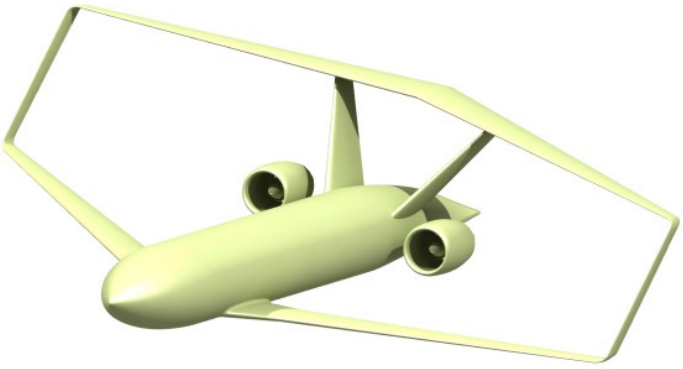

Figure 9. CAD model of the reference PrandtlPlane.

The designed configuration was available to be processed for detailed aerodynamic analysis. The high-fidelity aerodynamic assessment was performed by means of CFD simulations; drag polar curves were obtained by simulating the steady aerodynamics for different flight conditions, representative of the relevant operating conditions during the mission. The solver adopted was a steady compressible RANS with the *k*-*ε* turbulence

model; the volume mesh was composed of a prism layer of 20 layers with a growth rate of 1.1, and tetrahedral cells outside; the volume mesh size typically adopted was about 20 million cells for the half model, as a symmetry condition with respect to the longitudinal plane was applied. The software used to perform the computations was ANSYS Fluent [68]. In Figure 10, an example of the surface mesh is represented, and in Figure 11, an example of postprocessing of results is proposed.

Figure 10. Surface mesh details (aircraft half-model).

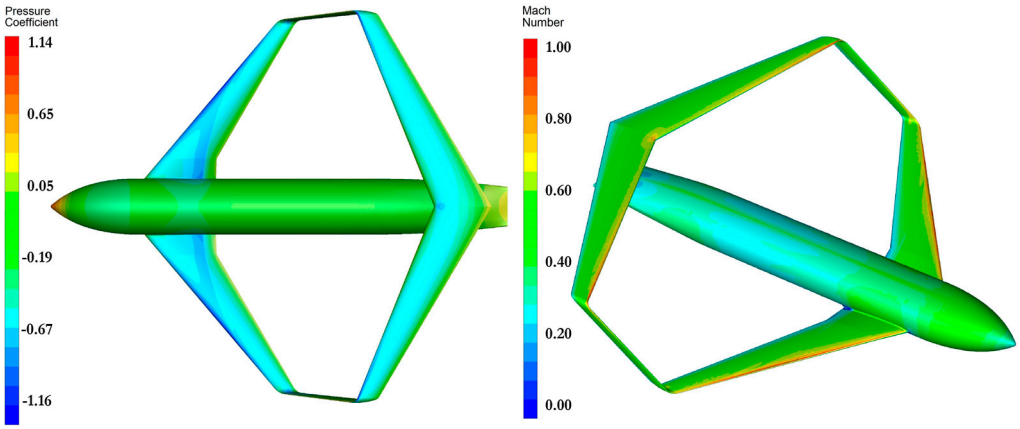

Figure 11. Example of postprocessing.

To reduce the computational cost, the component modelled was the wing–body assembly, while the drag of the vertical tails and engine nacelles were evaluated with the simplified models described in [53]. The solution chosen for the vertical tail assembly was a V-tail configuration; this has been shown to be necessary to alleviate potential flutter issues [69], as reported in [70–72]. This solution proved to be effective in meeting the flutter requirements in the case of the aircraft described in this article, as reported in [73]. The sizing of the V-tail was carried out with the aim of satisfying the directional stability requirements, as described in [74]; the flutter assessments were carried out subsequent to this sizing.

2.3.2. Structural Design and Mass Estimation

The mass breakdown was updated in this phase; in particular, the refinements regard the structural mass evaluation. As the simplified methods used to estimate the operating empty weight (and so also the structural weight) in the first two design stages are mainly referred to as statistical extrapolations concerning the structural data of classical aircraft architecture (tube-wing-tail), it was necessary to introduce specific physics-based models to evaluate the box-wing aircraft structural mass. The structural behaviour of a box-wing is very different from that of a conventional aircraft, concerning both the lifting system and fuselage structures. The main difference is related to the fact that the box-wing lifting system is over-constrained to the fuselage, as the main wing of a conventional aircraft is a statically determinate cantilevered lifting surface. The fuselage is a doubly supported beam in the case of a box-wing, borne in correspondence of the front and rear wing connections,

differently from the case of the conventional monoplane. To properly size and design the aircraft structural components, an in house-tool called WAGNER [75] was developed; the main goal of the WAGNER tool is to provide the preliminary structural design of the aircraft concerning the wings, the fuselage and the tailplanes' structural components. The sizing procedure relies on an FEM-based solver, namely the ABAQUS commercial software [76]; the WAGNER tool provides the automatic generation of the 3D geometry of the aircraft structures and the mesh of the structural components, such as stringers, frames, ribs, pressurisation bulkheads, floor beams and struts (Figure 12); the load cases' setting and computation through an ABAQUS solver (Figure 15); and the postprocessing of the results (Figure 16).

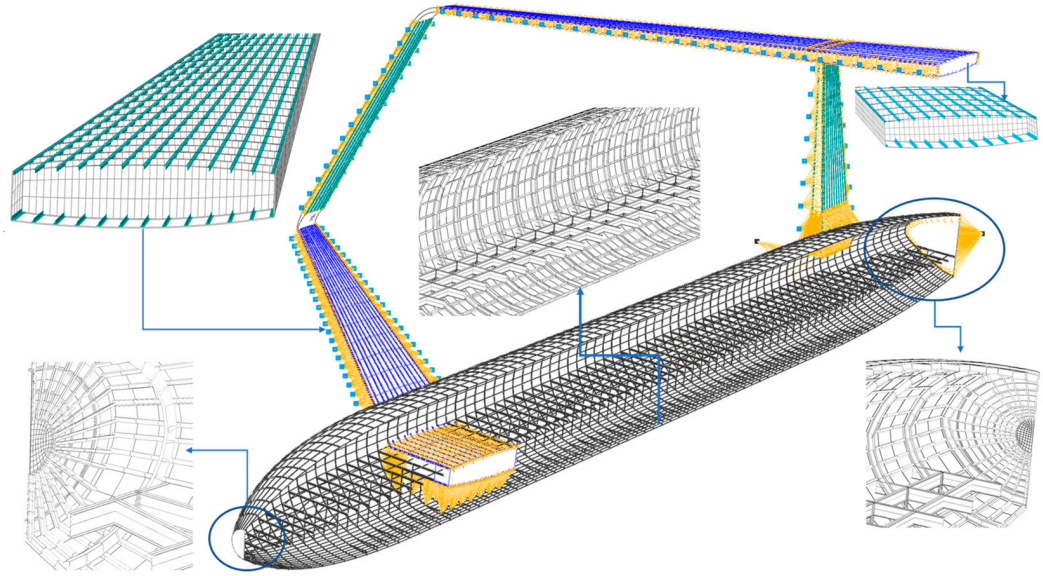

Figure 12. Typical Finite Element mesh of a PrP configuration (aircraft half-model) with some structural details.

The WAGNER code follows the sizing scheme reported in Figure 13; the main input is represented by the geometry from the *Level 1* block of the design process.

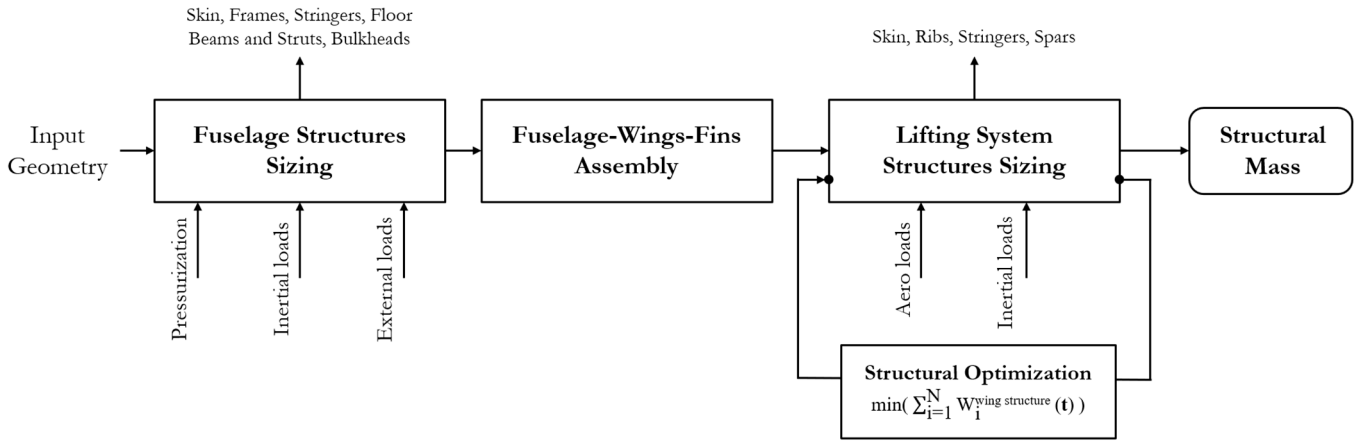

Figure 13. WAGNER structural sizing workflow.

The first step of the structural design workflow of Figure 13 provides the fuselage's structural sizing: the structure is modelled with shell elements for the skin, whereas stringers and frames are modelled with beam elements. The FE model of the fuselage is delimited by the end bulkheads, modelled as flat panels stiffened by beams in both radial (stringers) and circumferential (frame or ring) directions. Secondary structural parts of

the fuselage are considered as concentrated masses linked to the bulkhead structure (e.g., tail-cone) by means of multipoint constraints. Concentrated masses are also used to model landing gears and fuselage-mounted engines, connected to fuselage main frames. Finally, non-structural masses are spread over the mesh elements to account for the weight of payload, systems and operatings [63], as well as for doors, windows and special reinforcement structures [77,78].

Concerning the loading conditions for fuselage structural sizing, combined pressurisation and inertial loads are considered; limit and/or ultimate pressure are superimposed to gravity load related to load factor, n_z, ranging from -1 to +2.5. The sizing criterion is that the equivalent stress should be less than the allowable stress, with the latter being given by the yielding stress of the material divided by an appropriate safety factor, which usual standards require to be at least equal to 1.5. Figure 14 shows the global FE mesh of a half fuselage together with some example contour plots of stress and deformation induced by pressurisation and gravity loads.

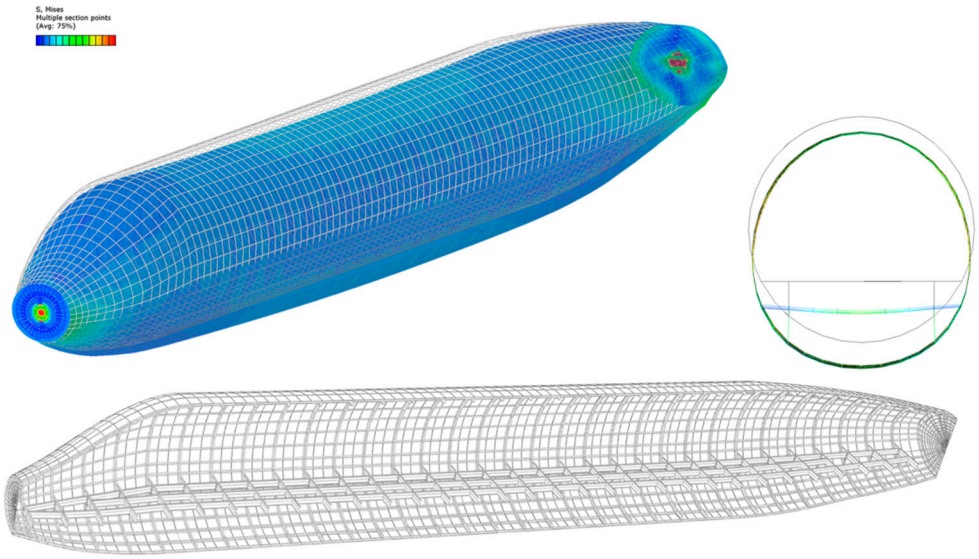

Figure 14. FE mesh of half a fuselage and example of contour plots of stress and deformation induced by ultimate pressurisation and gravity load with $n_z = +2.5$ (deformed scale factor: 20).

The second step concerns the assembly of the fuselage with the lifting system; the WAGNER software models the wings' geometry and meshes the structural components; the arrangement of structural components, such as frames and stringers pitch, is provided in input by reference cases available in literature for transport box-wing [79,80]; referring to Figure 12, the front wing is fixed to the fuselage by means of surface-based constraints; in particular, the spar webs (front and rear) are fixed to the main frames of the fuselage, while the ribs of the front wing are fixed to the floor beams. The same type of connection is used to attach the fin structure to the fuselage. Then, the lifting system structural sizing is performed; in particular, the wings' structural design is carried out by only considering static loads, according to a loading condition corresponding to a pull-up manoeuvre in cruise (M = 0.79, h = 11,000m, n_z = 2.5, $W = MTOW$); qualitatively, two constraints are imposed into the sizing procedure: (1) the wing-tip deflection, intended as the maximum deflection occurring in one of the main wings, should be such that large displacements are avoided; (2) the structure must support the limit load (given as a combination of aerodynamic and gravity loads) within the elastic field, so the equivalent Von Mises stress in both wings is constrained to be lower than the yielding stress of the material (divided by a safety factor) [81]. The aerodynamic loads, such as the spanwise lift distribution on the lifting surfaces, are provided as inputs from the AVL code. The wing structural sizing process is integrated into an optimisation procedure; the objective function is the structural mass of the lifting systems, $W^{wing\ structure}$ (Equation (23)); the constraints are those related

to structural stiffness, expressed as a maximum limitation on wings' tip displacement, δ_i^{tip} (Equation (24)), and structural strength, expressed as maximum limitation on the equivalent stress, σ_i^{eq} (Equation (25)), for the i-th wing; the design variable is the vector $\boldsymbol{t}$ of the thicknesses of the k-th structural component of the i-th wing t_{ik} (Equation (26)).

- Objective function

$$\min\left(\sum_{i=1}^{N} W_i^{wing\ structure}(\boldsymbol{t})\right) \tag{23}$$

- Stiffness constraint

$$\delta_i^{tip}(\boldsymbol{t}) \leq \delta_{MAX}^{tip} = k_{tip}\frac{b}{2} \tag{24}$$

- Strength constraint

$$\sigma_i^{eq}(\boldsymbol{t}) \leq \sigma_{MAX}/k_{SF} \tag{25}$$

- Design variables

$$\boldsymbol{t} = t_{ik} \tag{26}$$

- Design space

$$t_{\min} < t_{ik} < t_{MAX} \tag{27}$$

In Equation (24), the maximum wing tip displacement, δ_{MAX}^{tip}, is defined as a fraction, k_{tip}, of the half-wingspan, $b/2$; k_{tip} is considered equal to 0.1 for all the analyses carried out. In Equation (25), σ_{MAX} is fixed as equal to the yielding stress of the material, and k_{SF} is the safety factor; k_{SF} is set to 1.5. The wings are divided in a primary structure, i.e., the structure in which all the loads are concentrated, namely the wing-box consisting of upper/lower stiffened panels, spars, ribs, and in a secondary structure, mainly composed of components related to fixed leading/trailing structure and movables installation. The FEM-based sizing only involves the primary wing structure, as the secondary structures are evaluated by the method presented in [82] and are modelled in the FEM as distributed mass properly placed spanwise (Figures 15 and 16).

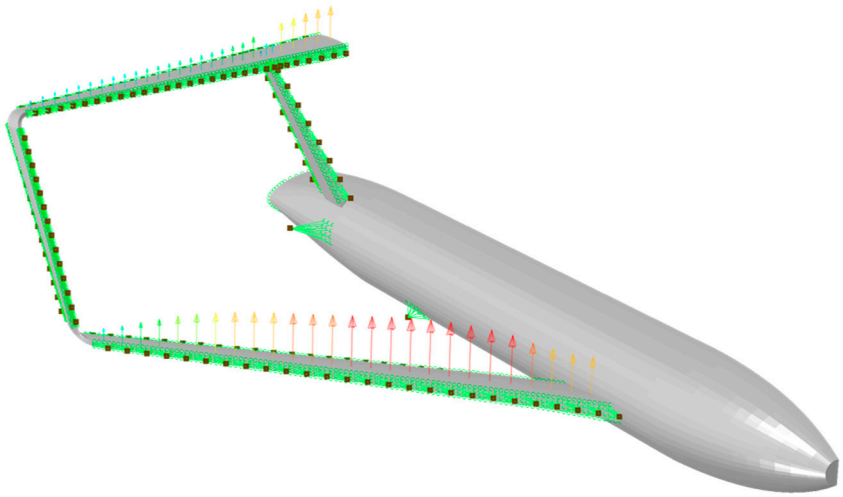

Figure 15. Secondary structures of the box-wing lifting system and aerodynamic forces (aircraft half-model).

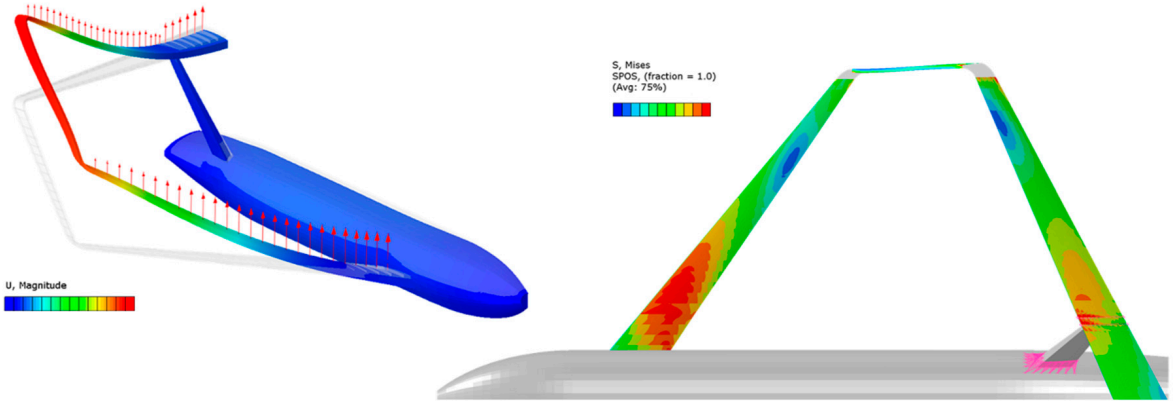

Figure 16. Example of deformed shape of the PrP configuration and Von Mises stress on both wings (aircraft half-model).

The output of the procedure is a complete structural mass breakdown of the main structures of the aircraft; the evaluation of non-structural components, i.e., cabin furnishings, on-board systems, etc., is performed in WAGNER by using the model described in [63]. The final output of the WAGNER tool is represented by the total mass of the configuration and the related components' breakdown, the coordinates of centre of gravity and the components of the inertia tensor.

2.3.3. Mission Simulation

The information collected in the *Level 2* stage, concerning the refinement of the weight estimation and the aerodynamic performance assessment, are useful to integrate in an in-house-developed mission simulation tool; this simulator allows one to estimate relevant output regarding the aircraft mission performance; in particular, the main outputs achievable from the simulation are the range and the related fuel burnt, for every mission inside the payload-range envelope of the aircraft. The mission performance is computed by integrating the equation of motion of the aircraft [55,83]; the reference mission is divided into taxing, take-off, climb, cruise, descent and diversion (Figure 17).

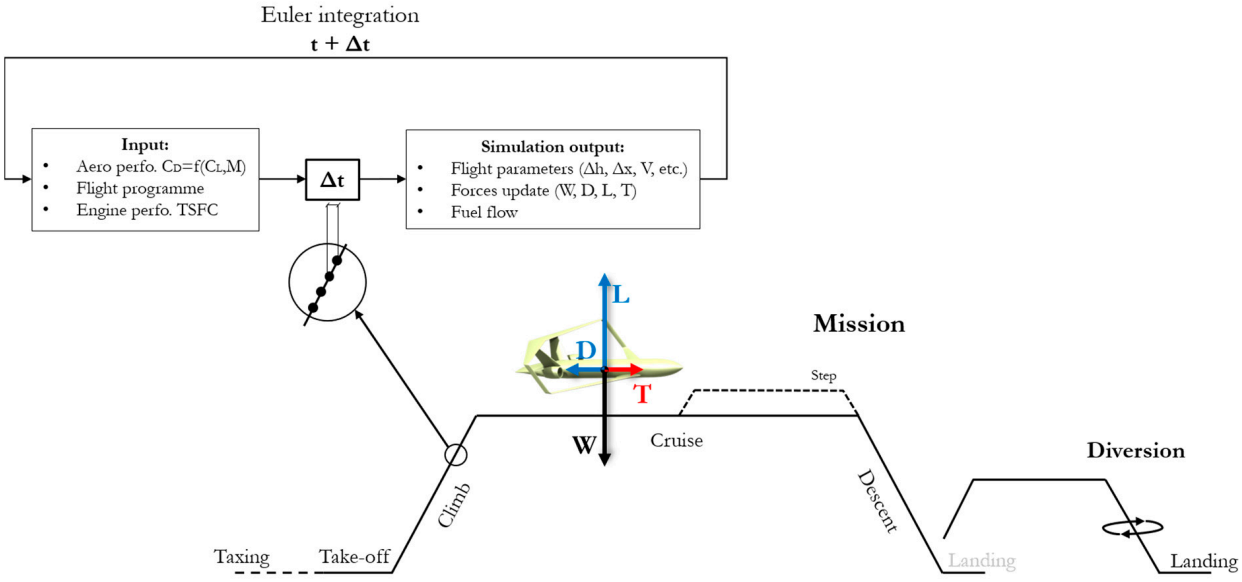

Figure 17. Mission simulation scheme.

Each mission segment is subdivided in timesteps Δt; the equations of motion are integrated by using the Euler algorithm, as reported in Equation (28) for a generic parameter k:

$$k(t + \Delta t) = k(t) + \dot{k}(t)\Delta t \tag{28}$$

The inputs for the simulation process are, for each time step: the aircraft's aerodynamic performance, expressed as response surfaces of the drag as a function of lift and flight condition ($C_D = f(C_L, M)$, derived by the CFD simulations results); the initial mass breakdown, depending on the payload and on the initial fuel mass; the flight programme for each mission segment; the main performance of the propulsion system, namely the thrust specific fuel consumption, *TSFC*. The simulation models used for each mission stage are briefly described in the following:

- The taxing fuel consumption is extrapolated by the data reported in [84]. The take-off phase was simulated by integrating the equation of motion of the aircraft in the longitudinal plane, also considering its pitch dynamics; the take-off simulation and analysis procedure used in this work is widely described in [85];
- The climb phase was simulated by integrating the equation of motion of the aircraft considered as a point mass in the longitudinal plane:

$$\tan\gamma = \frac{T - D}{L} \tag{29}$$

$$\dot{x} = V\cos\gamma \tag{30}$$

$$\dot{z} = V\sin\gamma \tag{31}$$

$$\dot{W} = -TSFC\,T \tag{32}$$

The climb programme was set as suggested in [86], namely by dividing the climb into segments flown at constant IAS or Mach number; the reference climb programme selected is "250 kt/300 kt/M_{cruise}". According to this programme: (1) the aircraft flies at IAS equal to 250 kt until it reaches an altitude of 10,000 ft; (2) the aircraft accelerates in an almost level flight until the IAS is 300 kt, and then flies at this speed until the crossover altitude (the crossover is defined as the altitude where the current Mach reaches the target cruise Mach); (3) the aircraft flies at a constant Mach number until it reaches the cruise altitude. During the climb, the aircraft changes its altitude, so its TAS increases as depicted in Figure 18 (left); an example of the aircraft climb trajectory is depicted in Figure 18 (right).

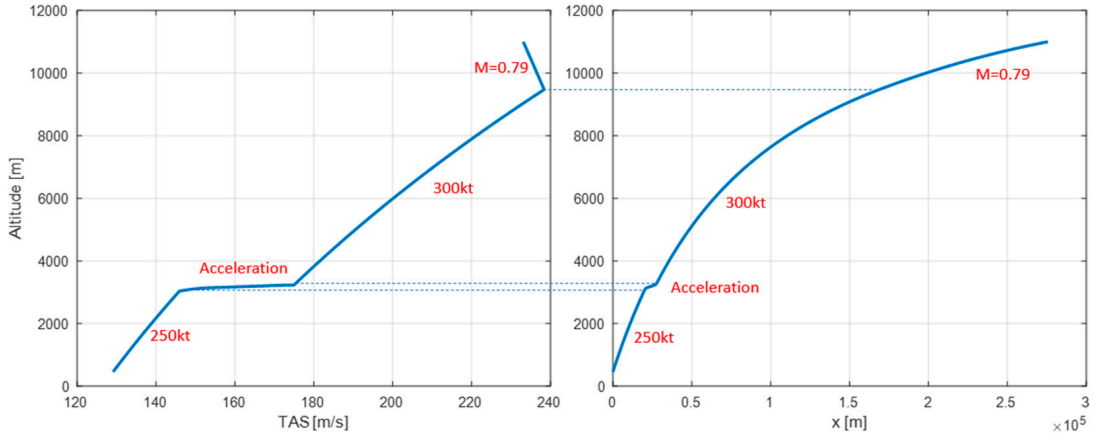

Figure 18. Reference climb programme.

- The cruise phase was simulated by integrating the equations of steady and level flights for the aircraft point mass model (Equations (33)–(35)); a constant altitude ($\dot{z}$) = 0 and constant speed ($\dot{x} = V$ = constant) flight programme was considered; the simulation, taking aircraft aerodynamic performance and cruise length into account, provided stepped cruise programmes if it resulted in performance gains.

$$L = Wg \tag{33}$$

$$T = D \tag{34}$$

$$\dot{W} = -TSFC\, T \tag{35}$$

- The descent starts at the cruise altitude and ends at an altitude of 1500 ft; the equations of motion are obtained for the climb, and in the same manner, the flight programme for the descent is made by segments at constant IAS or Mach number [85]; the reference selected programme is "M_{cruise}/300 kt/250 kt", namely: (1) the aircraft flies at a constant Mach number from the cruise altitude to the crossover altitude; (2) the aircraft flies at IAS = 300 kt from the crossover altitude to an altitude of 10,000 ft; (3) the aircraft decelerates in an almost level flight until the IAS is 250 kt, and then flies at this IAS until an altitude of 1500 ft is reached.
- Concerning diversion and loiter, analogous considerations about climb, cruise and descent were implemented.

3. Results of the Design Process

3.1. Input Data

The design methodology described in Section 2 was applied to the design case of a box-wing transport aircraft; in particular, the specific case of the PARSIFAL project [74,87–89] is presented.

To initialise the whole design process, it is necessary to define the Top Level Aircraft Requirements (TLARs). For the case study, the main TLARs are summarised in Table 3.

Table 3. PrandtlPlane main TLARs.

Max n° of passengers	310
Design range	5000 km
Cruise Mach	0.79
Initial Cruise Altitude	11,000 m
Max Wingspan	36 m

The selection of TLARs for the PARSIFAL case is widely described in [90]; in particular, the aim of introducing the PrandtlPlane as an alternative to conventional tube-and-wing aircraft follows two main design drivers, provided by the forecasts for the commercial air traffic scenario of the future:

- A huge increase in air traffic, especially on short/medium routes (up to 5000 km) [8] is expected;
- At the same time, relevant problems of airport saturation are forecasted [11].

To address these contrasting objectives, the expected higher lifting capability of a box-wing architecture is exploited; in particular, the aim of this design study is to develop an aircraft with an increased payload (up to 310 passengers), but the with same overall dimensions (compatibly with airport apron constraints) of the conventional competitor currently operating in the sector of the medium routes (e.g., Airbus A320 family or Boeing 737 family). The maximum wingspan is limited to 36 metres, compatibly with the apron

constraint provided by the ICAO Aerodrome Reference Code "C" [91]. Moreover, as the main objective for the commercial aviation of the future is to drastically cut the noxious emissions, the result of this design will be satisfactory only if a significant pollutant emission reduction is provided; this is theoretically possible by exploiting the expected better aerodynamic performance of the box-wing system. To properly assess the performance comparison with a conventional aircraft, it is necessary to identify a proper benchmark; the conventional benchmark selected is the CeRAS CSR-01 [92], a short/medium-range aircraft developed in the framework of the project CeRAS ("*Central Reference Aircraft data System*", [93]); the CeRAS project provides an open-access platform in which designs, geometries, data and procedures relevant to the CSR-01 configuration (*CeRAS Short Range version 01*, Figure 19) are collected. The CeRAS CSR-01 is a virtual simulacrum of an aircraft similar to the Airbus A320 [94] in terms of key features (Table 4), dimensions, payload and utilisation.

Figure 19. CeRAS CSR-01 configuration.

Table 4. Main features of the CeRAS CSR-01.

Ref. wing area	122.4 (+32.2 *) m^2
Design range	5000 km
Max n° pax	186
Wingspan	34.1 m
Fuselage length	37.5 m
Cruise altitude	11,000 m
Cruise Mach	0.79

* Horizontal tail.

3.2. Conceptual Design and Reference Layout Selection

As the TLARs for the box-wing design have been defined, the first level of the design process is performed, providing the fuselage design and the general information to initialise the aerodynamic optimisation in the *Level 1* block of the design process (Figure 2). Concerning the fuselage design, the focus is mainly on the external shape, the cabin section layout and the internal arrangement, as the main design driver is represented by the target number of passengers. For the PARSIFAL case study, the fuselage of the box-wing aircraft was selected with the following main features: a double-aisle cabin section was selected, with a 2-4-2 seats layout (Figure 20(left)); the fuselage length is set equal to 44.2 m, similar to the longest fuselage of a competitor operating in the medium range sector (Airbus A321); the cabin section external shape is near-elliptical, following the studies provided in [95]. This fuselage, arranged in a high-density layout, is able to transport a number of passengers equal to 308 (Figure 20 (right)).

Previous designs of wide body fuselage for box-wing aircraft were proposed in [40,96,97]; however, in the case of PARSIFAL, some actions to prevent penalisations in terms of turnaround time with respect to conventional competitors were provided, such as the introduction of enlarged aisles and of an extra boarding/de-boarding path; both

these aspects are highlighted in Figure 21, and their effects on turnaround time are widely discussed in [98,99]. In particular, the data provided by the simulations described in [98,99] show that the introduction of the PrP in the same sector as the A320-type aircraft implies a slight increase in turnaround time (+11% outstation, +25% full service) against a relevant increase in payload capacity (+66% passengers, +71% containers); these results were obtained by considering the same apron space (ICAO Code "C") for the two aircraft. The abovementioned simulations take all the main aspects of airport operations into account, from passenger arrival at the terminal to aircraft take-off.

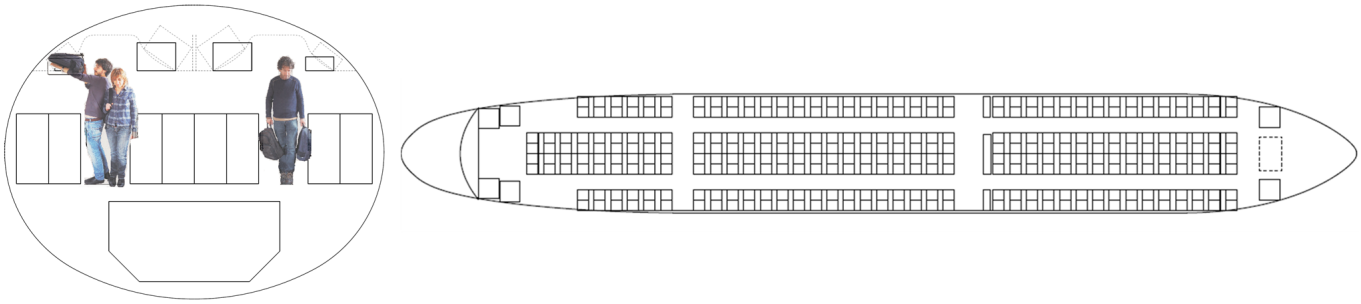

Figure 20. Cabin section layout (**left**); cabin arrangement (**right**).

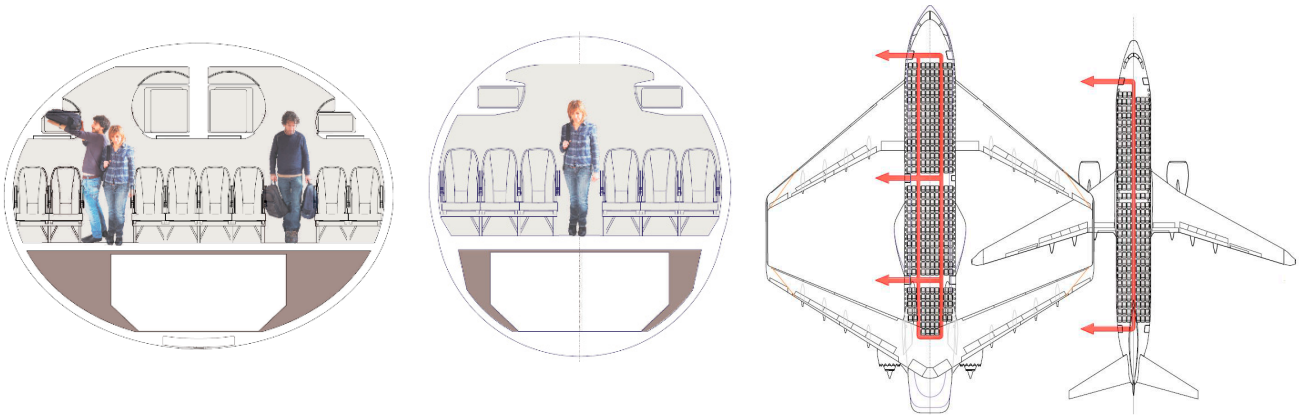

Figure 21. Cabin layout comparison between the PARSIFAL solution and a conventional single-aisle aircraft.

Once the fuselage is defined, the next step required to initialise the design process (*Level 0*) is to identify the main characteristics of the lifting system to apply simplified models for the estimation of the aerodynamic performance; to define an initial study case, a wing loading similarity was set between the box-wing and the CeRAS: in particular, to define the initial lifting system surface, the same wing-loading of the CeRAS was selected for the box-wing. By using this assumption in the relations of Equations (1), (4) and (6) for the initial aerodynamic evaluations and Equation (9) for the rough weight estimation, as described in Section 2.1, the data were obtained as input to initialise the second stage of the design process (*Level 1*). In this phase, several layouts of the box-wing aircraft were evaluated by means of the aerodynamic optimisation described in Section 2.2; at the end of the process, the output selected for the final performance analysis is represented by the configuration reported in Figure 22, whose main features are described in Table 5.

As detailed aspects related to the aeromechanical analysis of the box-wing aircraft may be out of the context of this paper, it is worth noting that such aspects have always been taken into account during the development of the aircraft. Specifically, general aspects of aeromechanical behaviour in the longitudinal plane of box-wing aircraft are extensively reported in [87]; a detailed summary of the design of the lifting system, with a focus on stability and controllability requirements, is given in [56]. The methods used to assess the aeromechanical characteristics of box-wing aircraft are extensively reported

in [87]; the approach used in the study involves a multi-fidelity approach, starting from the use of literature models [100], passing through extensive analysis campaigns with VLM solvers [58,74], up to the verification of requirements with CFD [74,88].

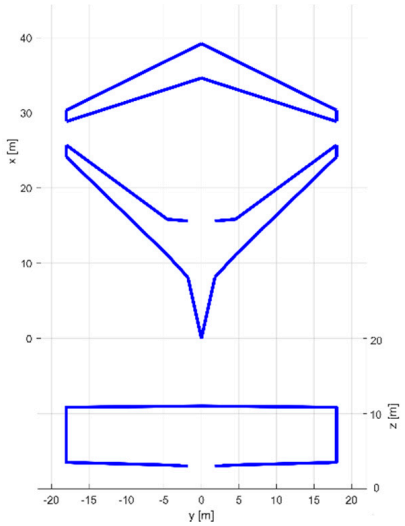

Figure 22. Reference box-wing layout.

Table 5. Main features of the reference box-wing.

@ Design Point	
M	0.79
h_{in}	11,000 m
L/D	21.62
C_L	0.4473
C_D	0.02068
$(L/S)_{front}$	604 kg/m^2
$(L/S)_{rear}$	477 kg/m^2
$(L/S)_{rear}/(L/S)_{front}$	0.789
SSM	0.10

It is worth pointing out the result concerning the wing loadings ratio $(L/S)_{rear}/(L/S)_{front}$ reported in Table 5: this value is in agreement with what is reported in [58]: the parameter $(L/S)_{rear}/(L/S)_{front}$ is the key lever to provide the maximum aerodynamic efficiency for box-wing aircraft compatibly with the constraints of static longitudinal stability and pitch trim; the result is also in agreement with what is described in [101], i.e., it provides the maximum performance in terms of C_{Lmax} in clean conditions (unflapped) for box-wing lifting systems.

3.3. Mission Performance Analysis

The selected configuration was analysed through the *Level 2* block of the workflow of Figure 2, by evaluating the aerodynamic behaviour and the structural mass in a more refined way to properly analyse the mission performance.

The CFD simulation model presented in Section 2.3.1 was used to evaluate the box-wing aircraft aerodynamics in different flight conditions; in Figure 23, the wing–body aerodynamic efficiency curves (namely E = lift-to-drag ratio, L/D) versus the lift force generated are reported for four different flight conditions.

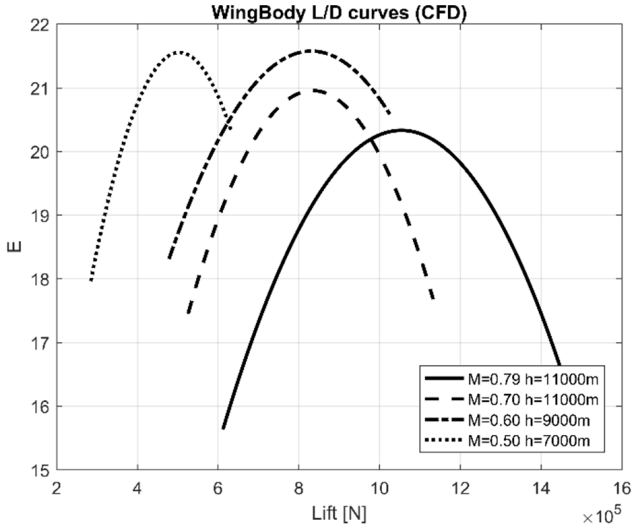

Figure 23. PrandtlPlane aerodynamic efficiency for different flight conditions.

Details of the aerodynamic performance in the cruise condition (M = 0.79 and h = 11,000 m) is reported in Figure 24; in particular, Figure 24 (left) reports the cruise aerodynamic efficiency for the wing–body assembly (CFD results) and for the whole configuration, including the estimation of the parasite drag of vertical tail planes and nacelles ([53] model); in this graph, some reference points are reported corresponding to the required lift to trim the aircraft in some reference conditions, to highlight the aerodynamic efficiency envelope of this configuration varying weight through the mission (MTOW = maximum take-off weight; ZFW = zero fuel weight, WOE = operating empty weight, LF = cabin load factor). In Figure 24 (centre) the C_D-C_L polar curve is reported, together with the breakdown of the C_D contribution of each aircraft component; Figure 24 (right) reports the viscous pressure breakdown of the polar curve.

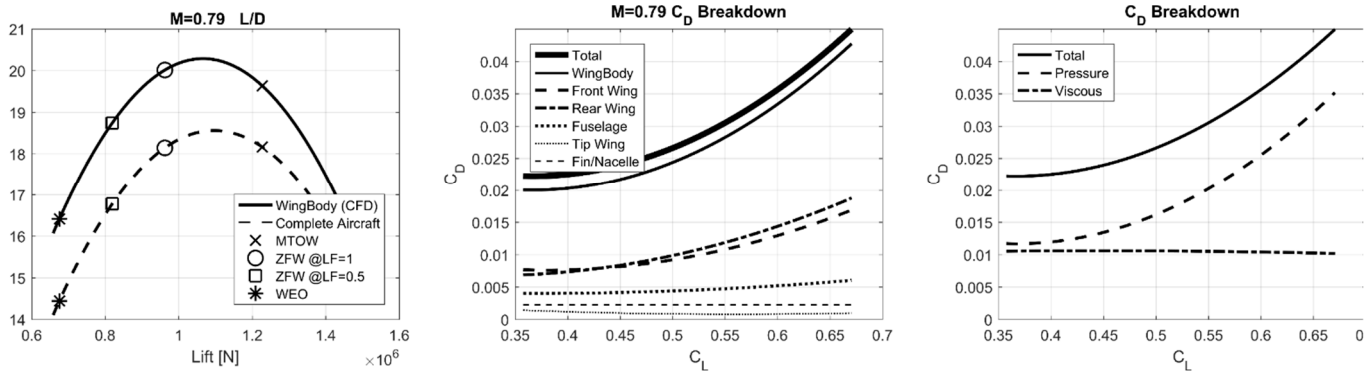

Figure 24. Details of the aerodynamic performance for PrandtlPlane in cruise condition; lift-to-drag curves (left), C_D breakdown -aircraft components- (centre), C_D breakdown -viscous/pressure- (right).

The second main input to the mission simulation platform is the mass breakdown of the aircraft; in the *Level 2* stage, the structural sizing has been performed through the FEM-based design and optimisation tool (Section 2.3.2); Table 6 reports the structural mass breakdown for the reference box-wing configuration.

Table 6. PrandtlPlane structural mass breakdown.

Component	Mass (kg)
Front Wing	7166
Rear Wing	6614
Vertical Tip-Wing	460
Fuselage	11,230
Vertical Tail Plane	1026

By calculating the other mass components as described in Section 2.3.2, the total mass evaluation of the reference box-wing conduces to a MTOW = 12,5126 kg, and a percentage repartition in components mass as reported in Figure 25; following the [63] model, the *Systems* category includes hydraulic, electric, pneumatic, fuel, engine, air conditioning, anti-ice, flight control, load systems, APU, avionics and instruments; *Operatings* includes cabin furnishings, cabin crew, crew seats, passengers seats, catering, emergency equipment, toilet fluid, oil and documentation.

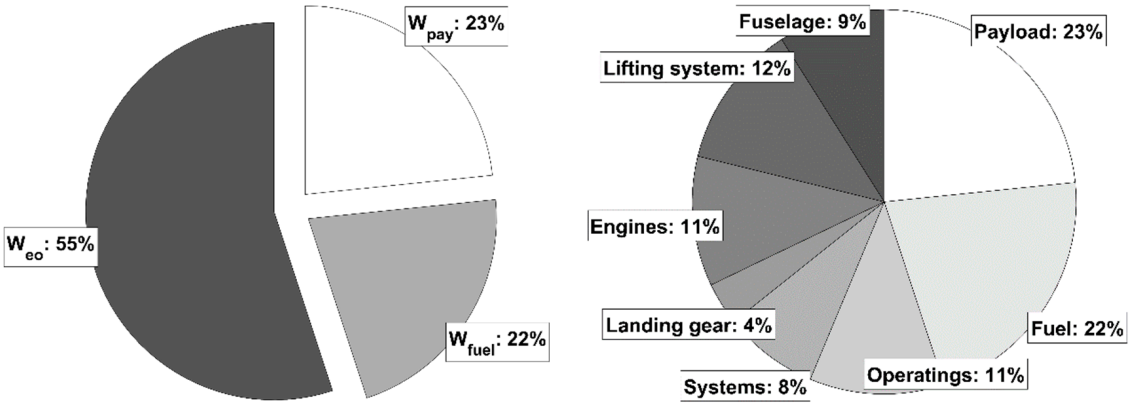

Figure 25. PrandtlPlane mass breakdown: general (**left**), components detail (**right**).

The information on the aerodynamic performance and weight of the aircraft are necessary to perform the mission simulations by means of the model described in Section 2.3.3. The simulations allow one to compute the mission performance of the reference box-wing; in particular, fuel burnt, range, flight time and other mission parameters such as time evolution of instant fuel consumption, speed, height, weight, etc., can be extracted from the simulation. Considering the box-wing harmonic mission, namely the mission with the maximum range at the maximum payload, the main results obtained are summarised in Table 7, and the main mission parameters are reported in Figure 26.

Table 7. Box-wing harmonic mission performance.

Number of passengers	308
Mission range	5722 km
Mission time	415 min
Mission fuel	21,844 kg
Total fuel	26,937 kg
Mission fuel per pax/km	0.01239 kg/km pax

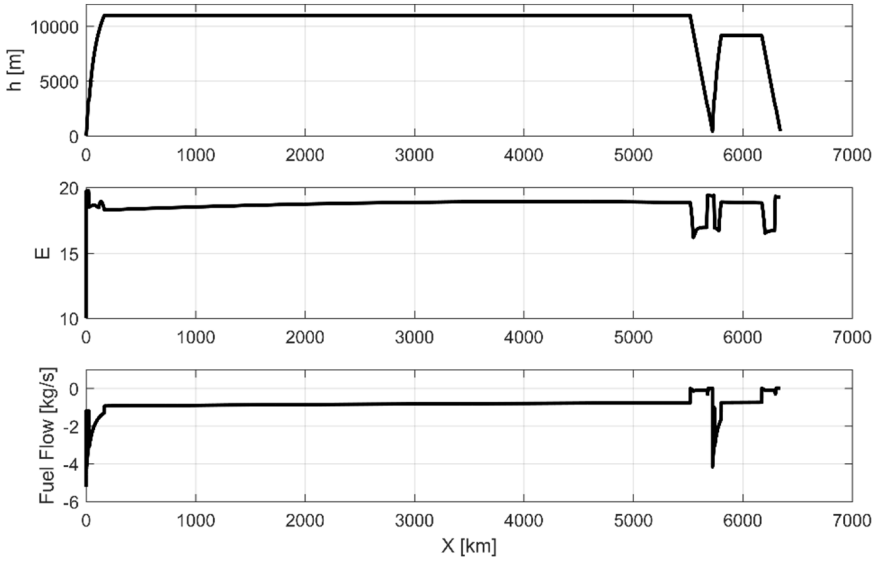

Figure 26. Box-wing harmonic mission height, aerodynamic efficiency and fuel flow evolution.

3.4. Box-Wing Performance Comparison with Respect to the Conventional Benchmark

The most relevant outcome of this work is the performance comparison between the unconventional PrandtlPlane aircraft and a conventional tube-and-wing benchmark. As reported in Section 3.1, the benchmark monoplane selected is the CeRAS CSR-01, a virtual mock-up of an Airbus A320-like aircraft, thus operating in the same routes of the reference box-wing; a top/front view comparison of the two aircraft is reported in Figure 27.

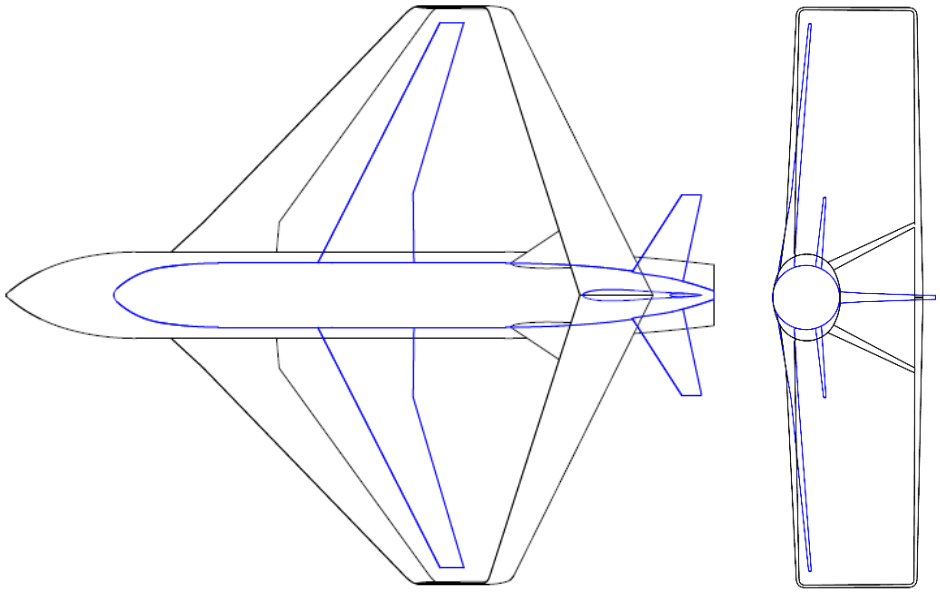

Figure 27. Views comparison between the PARSIFAL PrandtlPlane and the CeRAS conventional aircraft.

As far as the multilevel aircraft design and analysis diagram of Figure 2 is concerned, the activity on the CeRAS CSR-01 was limited to the *ANALYSIS* block, as the design and the geometrical characteristics of the aircraft are provided by the CeRAS database. Indeed, to make fair comparison between the box-wing aircraft and the benchmark monoplane, it is necessary to perform the aerodynamic, structural and flight analysis assessments with the same methods, tools and degree of fidelity. So, the same CFD analyses, the FEM based-structural sizing, the mass breakdown estimation and the mission simulation carried out for the box-wing aircraft were also performed for the CeRAS CSR-01. Figure 28 reports

the comparison of the aerodynamic performance of the two configurations: the wing–body aerodynamic efficiency (lift-to-drag ratio) curve trend with respect to the generated lift is reported in four flight conditions. Focusing on the cruise condition, namely at $M = 0.79$ and h = 11,000 m, it emerges that the box-wing aircraft is able to generate a larger amount of lift to trim larger weights, with a relevant increment in aerodynamic efficiency. Considering the point of maximum aerodynamic efficiency, the box-wing aircraft exhibits an increase in trim lift of +66% and a related increase in aerodynamic efficiency equal to +24%, while satisfying the same constraint on the maximum wingspan of the monoplane competitor.

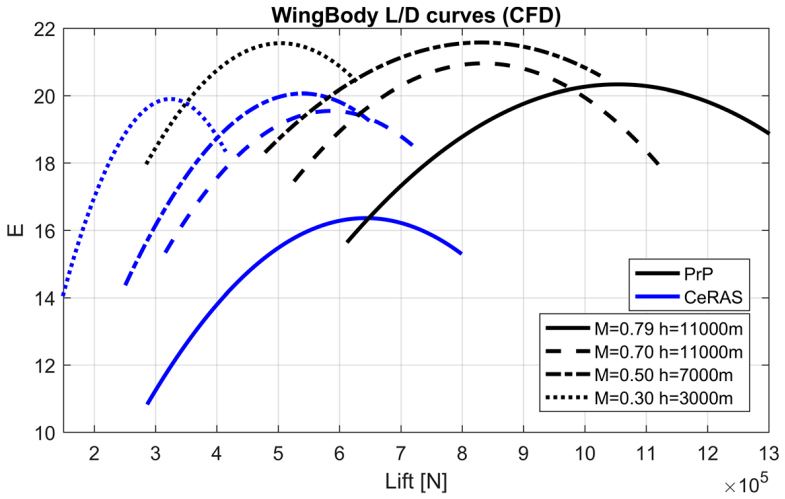

Figure 28. Comparison of aerodynamic efficiency curves: PrandtlPlane vs. CeRAS.

Figure 29 shows the detail of the operating points (from MTOW to W_{oe}) reported on the aerodynamic efficiency curves for both the configurations; the dashed curves represent the result corrected with the additional drag of fins and nacelles calculated by the approximate method [53].

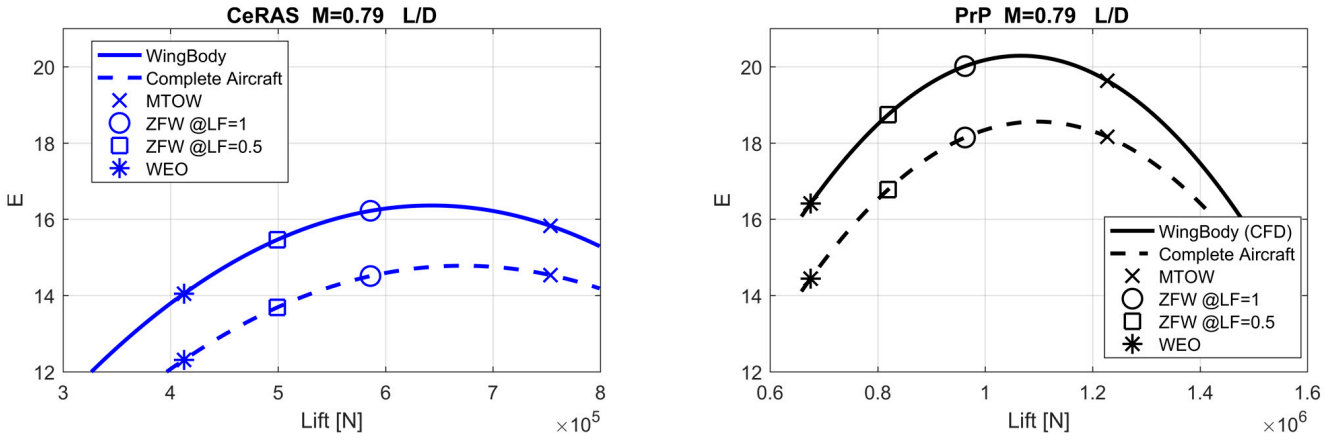

Figure 29. Detail of cruise aerodynamic efficiency for the PrandtlPlane and the CeRAS.

Figure 30 and Table 8 report the relevant data of the mass breakdown for the two aircraft; it is worth underlining that the fraction of the fuselage and lifting systems mass, together with the overall operating empty mass fractions, are very similar for the two configurations; the box-wing architecture does not introduce any significant penalisation in terms of structural mass with respect the conventional tube-and-wing solution.

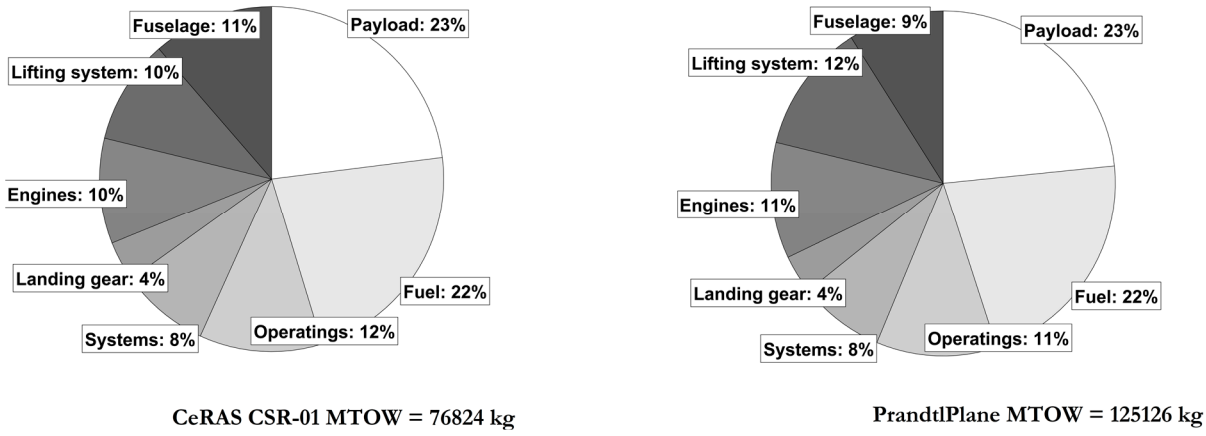

Figure 30. Components mass breakdown comparison.

Table 8. Mass breakdown comparison.

	CeRAS CSR-01	PrandtlPlane
W_{oe} (kg)	42,054	68,866
W_{oe}/MTOW	54.7%	55.0%
W_{fuel} (kg)	17,100	27,000
W_{fuel}/MTOW	22.3%	21.6%
W_{pay} (kg)	17,670	29,260
W_{pay}/MTOW	23.0%	23.4%
MTOW (kg)	76,824	12,5126

The information on aerodynamic performance and weights were used as input for the simulation of the harmonic mission of the CeRAS CSR-01 configuration; Table 9 reports the main data relevant to the CeRAS harmonic mission together with the mission data for the same range for the PrandtlPlane.

Table 9. Main mission data comparison.

	CeRAS CSR-01	PrandtlPlane
Number of passengers	186	308
Mission range	4790 km	4790 km
Mission fuel	13,670 kg	18,108 kg
Mission fuel per pax/km	0.01537 kg/km pax	0.01227 kg/km pax

The main outcome of this comparison is that the PrandtlPlane solution allows one to reduce the fuel consumption per passenger of a quantity equal to 20% with respect to CeRAS, if the CeRAS harmonic range is considered. It is worth stressing the fact that a conventional aircraft needs a larger wingspan to satisfy increases in MTOW as that exhibited by the PrP. On the other hand, the PrP, while having a higher payload capability and consequently a larger MTOW, has an advantage in fuel consumption per passenger–kilometre, although it does not demand more apron space than the conventional plane (CeRAS CSR-01).

Some relevant outputs of this mission simulation comparison, such as the flight trajectory, the mission aerodynamic efficiency and the instant fuel flow, are reported in Figure 31.

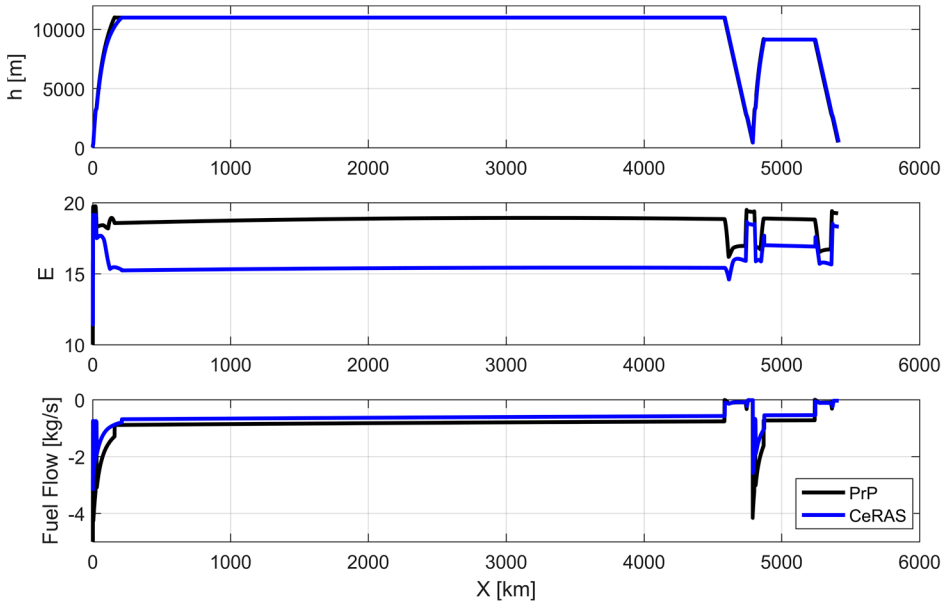

Figure 31. Comparison of flight trajectory, aerodynamic efficiency and fuel flow.

The same comparisons were performed by considering different missions, by varying the initial condition in terms of payload and target mission range. In particular, several missions were simulated by considering a variation of the mission range in the interval of [500 km–4790 km] (the upper bound is fixed equal to the CeRAS harmonic range) and by varying the cabin load factor (namely the number of boarded passengers divided by the maximum number of passengers) in the interval [0.5–1]. Figure 32 shows the comparison, in terms of percentage variation in the averaged mission aerodynamic efficiency (namely, lift-to-drag ratio); the gains for the PrandtlPlane with respect to the CeRAS are relevant in the whole considered envelope, as the increase in mean aerodynamic efficiency ranges from 15% up to 22%.

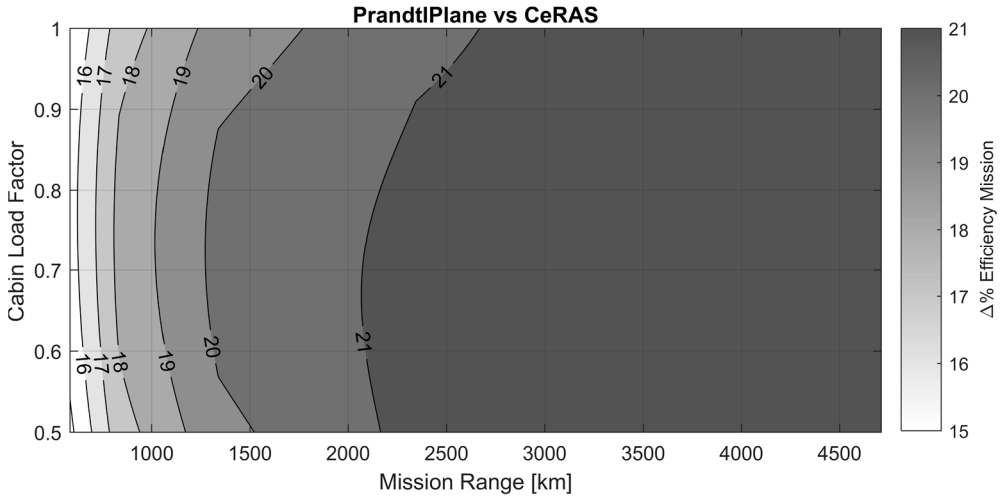

Figure 32. Comparison in terms of mean mission aerodynamic efficiency.

3.5. Box-Wing Operating Performance

In this section, a comparison between the PARSIFAL PrandtlPlane and the CeRAS CSR-01 conventional aircraft is presented in terms of a payload-range diagram. The payload-range diagram and the mission performance inside this envelope were calculated with the mission simulation tool described in Section 2.3.3. In Figure 33, the payload-range diagrams of the two aircraft are superimposed: it emerges that the PARSIFAL box-wing

aircraft covers a wider market space, in terms of the maximum number of passengers (+66%) and maximum achievable ranges, despite having the same wingspan constraints of the CeRAS CSR-01 aircraft (compatibility with ICAO Reference Aerodrome Code "C"), and so operating from the same airports and aprons.

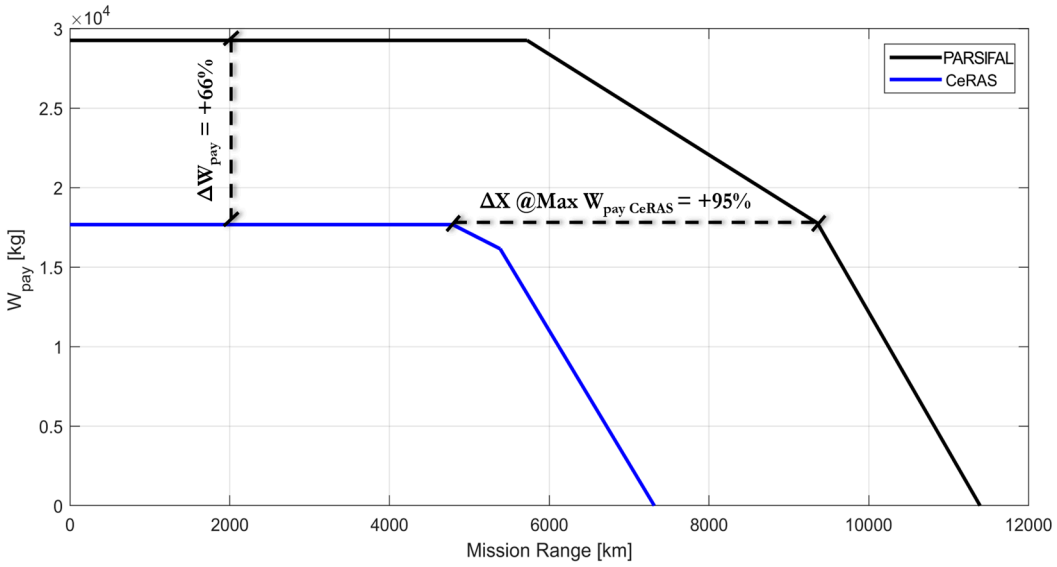

Figure 33. Comparison between the payload-range diagrams (PARSIFAL PrandtlPlane vs. CeRAS CSR-01).

In the PARSIFAL payload-range diagram reported in Figure 34, different and flexible utilisations of the box-wing aircraft are qualitatively described by highlighting the different covered market sectors; in particular, the introduction of the PrandtlPlane allows one to open a new market sector related to the short/medium-haul with an increased payload (the 'PARSIFAL area'); up today, this market sector is not covered by any conventional aircraft compliant with the ICAO Reference Code "C" wingspan constraint, and the upper limit to the maximum payload for this interval of mission lengths is represented by the Airbus A321. Moreover, the same box-wing aircraft satisfies the requirements of the so-called *Middle of the Market* sector [102] by transporting about 200 (250) passengers for 8900 (7400) kilometres. In addition, it is possible to transport a similar number of passengers of the CeRAS CSR-01 (configured in a high-density layout) for long range routes, up to 9350 km.

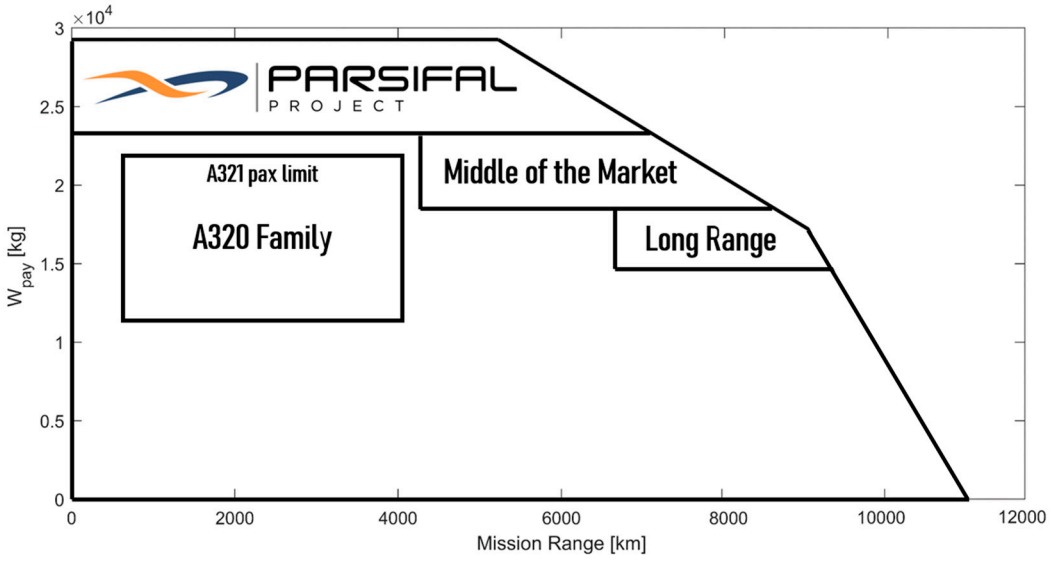

Figure 34. PARSIFAL PrandtlPlane payload-range diagram.

3.6. Discussion of the Performance Comparison between the Box-Wing and the Conventional Competitor

The information presented in Sections 3.4 and 3.5 can be combined in order to compare the two reference aircraft in terms of utilisation and mission performance. In particular, the superimposition of the contour map of the percentage variation of the mission fuel burnt per pax km with the payload-range diagram is shown in Figure 35. Keeping in mind the difference in terms of payload capacity between the two configurations (as described in Figure 33), in the following discussion, the presentation of the performance comparisons refers to the cabin load factor range graphs, to simplify the representation of the data presented, as reported in Figure 35.

The combined analysis of Figures 33 and 35 provides a complete overview of the performance comparison; it shows that:

- The PARSIFAL PrandtlPlane has a larger pax-range envelope with respect to the CeRAS CSR-01 monoplane; in particular, at the harmonic point, the PrandtlPlane presents +66% more passengers and +19% longer range. Both the aircraft are compliant with the ICAO Aerodrome Reference Code "C" constraint (max wingspan equal to 36 m);
- The PARSIFAL PrandtlPlane can transport the same maximum number of passengers of the CeRAS CSR-01 (186 pax in high density) for about 9350 km, 95% more than the reference aircraft.
- The PARSIFAL PrandtlPlane exhibits a gain in terms of mission fuel per pax km in the relevant area of the pax-range diagram, up to the harmonic range of the CeRAS CSR-01; considering the harmonic ranges, the PrandtlPlane needs 19% less fuel per passenger–kilometre; the reduction in fuel per passenger is relevant, from −13% up to −22%, in the whole operating space considered; this also reflects the aircraft environmental performance: the introduction of the PrandtlPlane configuration allows a reduction in pollutant and greenhouse gas emissions per passenger, as widely discussed in [99,103];

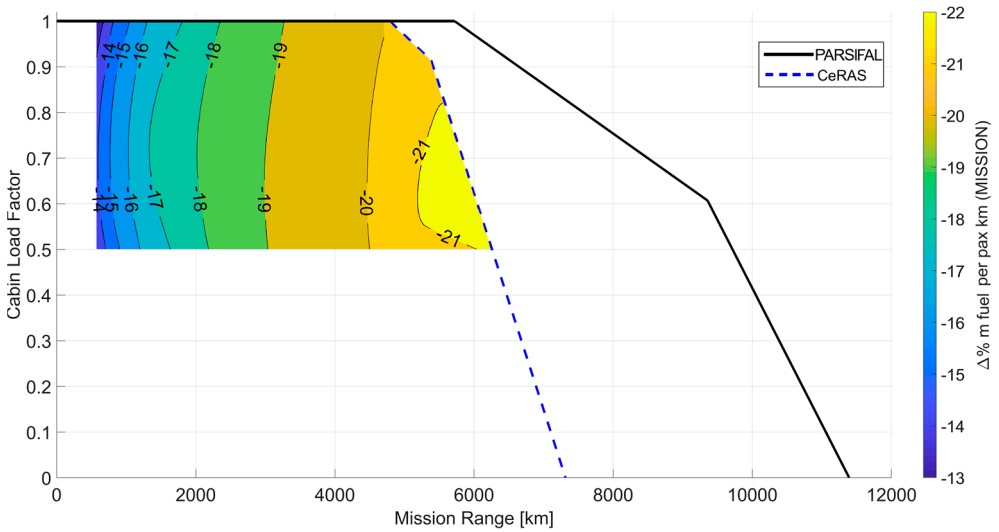

Figure 35. Comparison between the cabin load factor range diagrams (PARSIFAL PrandtlPlane vs. CeRAS CSR-01) and fuel consumption per pax km.

- The diagram in Figure 36 shows the contour maps of the percentage difference of the fuel consumption per passenger–kilometre for the two aircraft, both for the zone inside the CeRAS CSR-01 envelope and outside this limit, up to the CeRAS CSR-01 ferry range. It is clear that direct comparisons (i.e., with the same cabin load factor and range) can only be made within the limits of the CeRAS envelope; beyond this limit, the PARSIFAL PrandtlPlane can fly longer distances with the same cabin load factor, or have higher cabin load factors for the same range, with respect to the CeRAS competitor. In this area, the comparison in terms of fuel burnt per passenger–kilometre

cannot be made considering the same range and cabin load factor for the two aircraft; thus, the values obtained for PARSIFAL are compared with those relevant to the best performance of CeRAS, i.e., the missions at the border of the envelope (maximum cabin load factor for each considered range). As a result, the comparisons are carried out considering a same range for the two aircraft, but with different cabin load factors. In this zone of the diagram, the higher fuel efficiency of the PARSIFAL PrandtlPlane is combined with the capability to fly with higher cabin load factors for the considered ranges, and therefore the reduction in fuel consumption per passenger–kilometre increases very sensitively as the range increases, as shown in Figure 36.

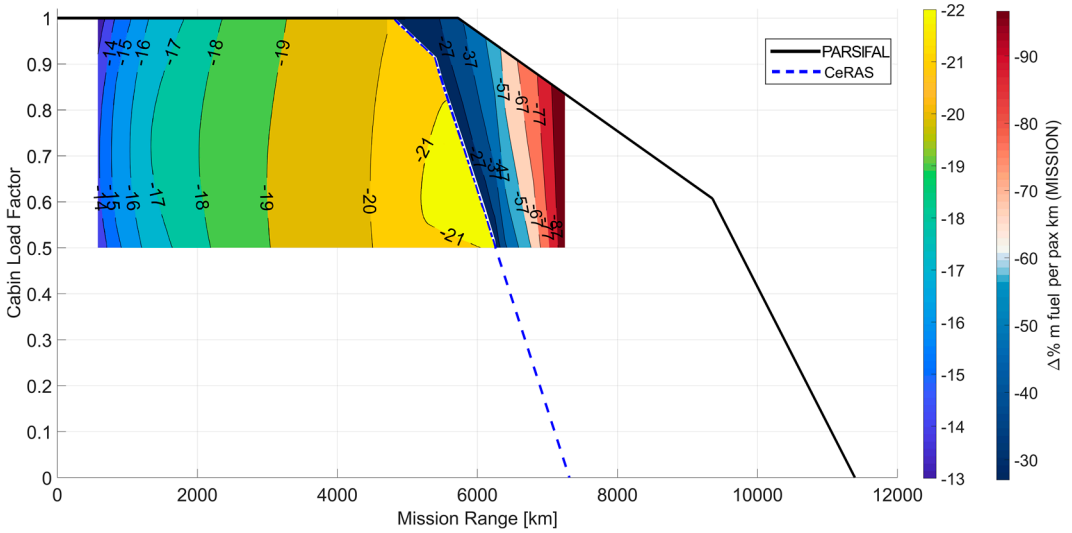

Figure 36. Overview of the comparison (PARSIFAL PrandtlPlane vs. CeRAS CSR-01) of the fuel per passenger–kilometre and cabin load factor range diagrams, up to the CeRAS ferry range.

- In the area of the cabin load factor range diagram beyond the ferry range of the CeRAS CSR-01 configuration, it is not possible to make comparisons in terms of fuel consumption. This region is highlighted in amaranth in the diagram of Figure 37. The PARSIFAL PrandtlPlane, with the same constraints on maximum wingspan of the reference monoplane competitor, is able to fly longer routes with a number of passengers comparable to the CeRAS CSR-01, thus offering an additional advantage in terms of operational flexibility.

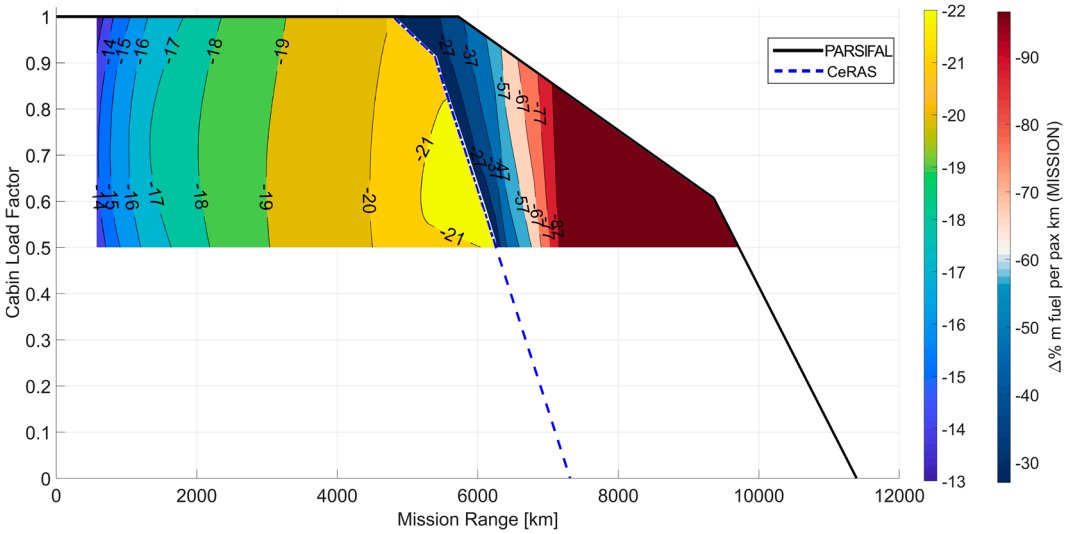

Figure 37. Overview of the comparison (PARSIFAL PrandtlPlane vs. CeRAS CSR-01) of the fuel per passenger–kilometre and cabin load factor range diagrams, beyond the CeRAS ferry range.

4. Conclusions

This paper described the potential effects of the introduction of PrandtlPlane aircraft in the short/medium-haul air traffic sector. The characteristics of this unconventional configuration, which is based on a box-wing lifting system, allow an increase in payload capability, without the need to increase the overall size of the aircraft compared to competitors in the same sector. Furthermore, the features of the lifting system enable the enhancement of the aerodynamic performance, in particular in terms of the lift-to-drag ratio, and therefore to achieve benefits in terms of reduction in fuel consumption per passenger. The introduction of this disruptive configuration is thus a possible solution to the main challenges of aviation in the near future, namely: the need to reduce pollutant and climate-changing emissions; the need to satisfy an expected growth in air traffic demand, especially on short/medium routes; and the need to alleviate problems of congestion and saturation of airport areas.

Since the aerodynamic benefits may be reduced when a new configuration is assessed from the point of view of other disciplines, a multidisciplinary design and analysis methodology was developed and used to develop a reference box-wing aircraft, and to analyse its operational potential and its performance. This methodology was structured with an increasing fidelity strategy, by using progressively more reliable design and analysis tools, with the aim of obtaining the best preliminary performance assessment. A conventional benchmark aircraft was identified to carry out the performance comparison; the selected aircraft was the CeRAS CSR-01, a virtual aircraft mock-up with characteristics similar to an Airbus A320.

The analysis and performance comparison was carried out with the same procedures and tools for the two considered configurations. The results obtained proved that the PrandtlPlane aircraft is able to carry 66% more passengers than the conventional benchmark, while maintaining the same dimensional constraints, hence keeping the possibility of operating from the same airport aprons. In addition, the PrandtlPlane is able to carry the same maximum payload as the CeRAS CSR-01 for up to 95% longer routes and, more importantly, it is able to reduce the fuel consumption per passenger over the whole envelope of the operational missions of interest. In particular, the maximum reduction in fuel consumed per passenger transported was quantified as 22%, when considering the typical operational missions of the CeRAS CSR-01. Finally, this paper shows how the box-wing architecture confers, to aircraft with the typical dimensions of short-to-medium range, the capability to cover additional sectors of the air transport market, such as *Middle of the Market* and long range.

The multidisciplinary design and analysis methodology presented in this paper can be applied to box-wing aircraft of various categories; further investigations will concern the development and the performance analysis of box-wing aircraft for the regional and commuter classes. In addition, the modularity and the flexibility of the design workflow allows the efficient integration of additional design elements, such as the introduction of hybrid-electric powertrains, or the inclusion of analysis and design methodologies of increasing fidelity, such as CFD-driven shape optimisation. Studies concerning the manufacturability and assembly of the box-wing aircraft are also worthy of further investigation: a step forward has been made concerning the actual benefits deriving from the operability of the box-wing, but there is still uncertainty regarding the possibility of setting up effective assembly lines. Investigating this topic may represent a further step towards the actual introduction of box-wing aircraft in the transport aviation sector.

Author Contributions: Conceptualisation, K.A.S. and V.C.; methodology, formal analysis, investigation, K.A.S., V.C., G.P., V.B.; software, validation; resources, data curation, K.A.S., G.P., V.B., D.Z.; writing—original draft preparation, K.A.S., V.C.; writing—review and editing, G.P., V.B., D.Z.; visualisation, K.A.S., G.P.; supervision, project administration, funding acquisition, V.C. All authors have read and agreed to the published version of the manuscript.

Funding: This research was funded by the European Union under the Horizon 2020 Research and Innovation Program (Grant Agreement n.723149).

Data Availability Statement: The data presented in this study are available on request from the corresponding author.

Acknowledgments: The present paper concerns part of the activities carried out within the research project PARSIFAL ("Prandtlplane ARchitecture for the Sustainable Improvement of Future AirpLanes"), which has been funded by the European Union under the Horizon 2020 Research and Innovation Program (Grant Agreement n.723149).

Conflicts of Interest: The authors declare no conflict of interest.

Abbreviations

The following abbreviations have been used in the paper:

APU	Auxiliar Power Unit
AR	Aspect Ratio
AVL	Athena Vortex Lattice
CAD	Computer Aided Design
CeRAS	Central Reference Aircraft Data System
CFD	Computational Fluid Dynamics
CSR	CeRAS Short Range
FEM	Finite Element Method
IAS	Indicated Air Speed
ICAO	International Civil Aviation Organization
LF	Load Factor (passenger cabin)
MTOW	Maximum Take-Off Weight
PrP	PrandtlPlane
RANS	Reynolds Averaged Navier–Stokes equations
SSM	Static Stability Margin
TLARs	Top Level Aircraft Requirements
TSFC	Thrust Specific Fuel Consumption
VLM	Vortex Lattice Method

Symbols

The following symbols have been used in the paper:

b	Wingspan	m
c	Chord	m
C_D	Drag coefficient	
C_{D0}	Parasite drag coefficient	
C_{Di}	Induced drag coefficient	
C_{Dwave}	Wave drag coefficient	
$C_{D\,foil}$	Airfoil drag coefficient	
$C_{D\,tot}$	Total drag coefficient	
C_f	Friction coefficient	
C_{fe}	Equivalent skin friction coefficient	
C_L	Lift coefficient	
C_l	Section lift coefficient	
C_M	Pitch moment coefficient	
d	Diameter	m
D	Drag	N
e	Oswald factor	
E	Aerodynamic efficiency (Lift to Drag ratio)	
FF	Form factor	
$\boldsymbol{g}$	Inequality constraint	
g	Gravity acceleration	m/s^2
h	Altitude	m
h/b	Wings height to span ratio	
k	Polar drag coefficient	
k_{tip}	Stiffness constraint factor	

k_{SF}	Strength constraint safety factor	
l	Length	m
L	Lift	N
lb	Lower boundary	
L/S	Lifting surface wing loading	kg/m^2
M	Mach number	
n_z	Vertical load factor	
Q	Interference factor	
$S_{exposed}$	Planform area of the wing exposed to the flow	m^2
S_{ref}	Reference surface	m^2
S_{wet}	Wetted surface	m^2
$\boldsymbol{t}$	Vector of thicknesses of structural wingbox components	mm
t/c	Thickness to chord ratio	
T	Thrust	N
ub	Upper boundary	
V	Speed	m/s
W	Weight	kg
W_{des}	Design weight	kg
W_{oe}	Operating empty weight	kg
$\boldsymbol{x}$	Design variables vector	
x	Aircraft longitudinal position	m
x_{LE}	Longitudinal leading edge coordinate	m
y	Spanwise coordinate	m
z	Aircraft vertical position	m
α	Angle of attack	deg
γ	Trajectory slope	deg
δ_{tip}	Wing tip displacement	mm
ε	Tolerance	
θ	Section twist	deg
λ	Taper ratio	
Λ	Sweep angle	deg
σ_{eq}	Equivalent stress	MPa

Other subscripts:

comp	Component
cruise	Cruise
cyl	Cylinder
eng	Engine
front	Front wing
fus	Fuselage
fuel	Fuel
max	Maximum
min	Minimum
oper	Operating items
pay	Payload
rear	Rear wing
root	Root section
sys	On board systems
TH	Threshold
tip	Tip section
trim	Trim condition
vertical	Vertical tail
wing	Wing

References

1. Lee, D.S.; Fahey, D.W.; Forster, P.M.; Newton, P.J.; Wit, R.C.; Lim, L.; Owen, B.; Sausen, R. Aviation and global climate change in the 21st century. *Atmos. Environ.* **2009**, *43*, 3520–3537. [CrossRef]
2. Lee, D.S.; Pitari, G.; Frewe, V.; Gierens, K.; Penner, J.E.; Petzold, A.; Prather, M.J.; Schumann, U.; Bais, A.; Berntsen, T.; et al. Transport impacts on atmosphere and climate: Aviation. *Atmos. Environ.* **2010**, *44*, 4678–4734. [CrossRef] [PubMed]
3. Dessens, O.; Köhler, M.O.; Rogers, H.L.; Jones, R.L.; Pyle, J.A. Aviation and climate change. *Transp. Policy* **2014**, *34*, 14–20. [CrossRef]
4. Wuebbles, D. Evaluating the impacts of aviation on climate change. *Eos Trans. Am. Geophy. Union* **2007**, *88*, 157–160. [CrossRef]
5. Brasseur, G.P.; Gupta, M. Impact of aviation on climate. *Am. Meteorol. Soc.* **2016**, *97*, 561–583. [CrossRef]
6. Eurocontrol. European Aviation in 2040, Challenges of Growth, Annex 2, Adapting Aviation to a Changing Climate. 2018. Available online: https://perma.cc/842G-4A3R (accessed on 18 July 2021).
7. Eurocontrol. European Aviation in 2040, Challenges of Growth, Annex 1, Flight Forecast to 2040. 2018. Available online: https://perma.cc/YW6Y-JU7J (accessed on 18 July 2021).
8. PARSIFAL Project Consortium. Report on Socio Economic Scenarios and Expectations. PARSIFAL Project Deliverables, D 1.1. 2017. Available online: https://perma.cc/JYL5-K9ST (accessed on 18 July 2021).
9. Airbus. Cities, Airports & Aircraft—2019–2038. Global Market Outlook. 2019. Available online: https://perma.cc/WSW3-7JK5 (accessed on 18 July 2021).
10. Boeing. Commercial Market Outlook—2019–2038. 2019. Available online: https://perma.cc/WQ53-7WEB (accessed on 18 July 2021).
11. Eurocontrol. European Aviation in 2040, Challenges of Growth. 2018. Available online: https://perma.cc/2A2J-B7PW (accessed on 18 July 2021).
12. Schäfer, A.W.; Barrett, S.R.; Doyme, K.; Dray, L.M.; Gnadt, A.R.; Self, R.; O'Sullivan, A.; Synodinos, A.P.; Torija, A.J. Technological, economic and environmental prospects of all-electric aircraft. *Nat. Energy* **2019**, *4*, 160–166. [CrossRef]
13. Hoelzen, J.; Yaolong, L.; Bensmann, B.; Winnefiled, C.; Elham, A.; Fiedrichs, J.; Hanke-Rauschenbach, R. Conceptual design of operation strategies for hybrid electric aircraft. *Energies* **2018**, *11*, 217. [CrossRef]
14. Pornet, C.; Isikveren, A.T. Conceptual design of hybrid-electric transport aircraft. *Prog. Aerosp. Sci.* **2015**, *79*, 114–135. [CrossRef]
15. Palaia, G.; Zanetti, D.; Abu Salem, K.; Cipolla, V.; Binante, V. THEA-CODE: A design tool for the conceptual design of hybrid-electric aircraft with conventional or unconventional airframe configurations. *Mech. Ind.* **2021**, *22*, 19. [CrossRef]
16. Friedrich, C.; Robertson, P.A. Hybrid-electric propulsion for aircraft. *J. Aircr.* **2015**, *52*, 176–189. [CrossRef]
17. Brelje, B.J.; Martins, J.R. Electric, hybrid, and turboelectric fixed-wing aircraft: A review of concepts, models, and design approaches. *Prog. Aerosp. Sci.* **2019**, *104*, 1–9. [CrossRef]
18. Khandelwal, B.; Karakurt, A.; Sekaran, P.R.; Sethi, V.; Singh, R. Hydrogen powered aircraft: The future of air transport. *Prog. Aerosp. Sci.* **2013**, *60*, 45–59. [CrossRef]
19. Baroutaji, A.; Wilberforce, T.; Ramadan, M.; Olabi, A.G. Comprehensive investigation on hydrogen and fuel cell technology in the aviation and aerospace sectors. *Renew. Sustain. Energy Rev.* **2019**, *106*, 31–40. [CrossRef]
20. Nojoumi, H.; Dincer, I.; Naterer, G.F. Greenhouse gas emissions assessment of hydrogen and kerosene-fueled aircraft propulsion. *Int. J. Hydrogen Energy* **2019**, *34*, 1363–1369. [CrossRef]
21. Ng, W.; Datta, A. Hydrogen fuel cells and batteries for electric-vertical takeoff and landing aircraft. *J. Aircr.* **2019**, *56*, 1765–1782. [CrossRef]
22. Azami, M.H.; Savill, M. Comparative study of alternative biofuels on aircraft engine performance. *Inst. Mech. Eng. Part G J. Aerosp. Eng.* **2017**, *231*, 1509–1521. [CrossRef]
23. Moore, R.H.; Thornhill, L.; Weinzierl, B.; Sauer, D.; D'Ascoli, E.; Kim, J.; Lichtenstern, M.; Scheibe, M.; Beaton, B.; Beyersdorf, A.; et al. Biofuel blending reduces particle emissions from aircraft engines at cruise conditions. *Nature* **2017**, *543*, 411–415. [CrossRef] [PubMed]
24. Mazlan, N.M.; Savill, M.; Kipouros, T. Effects of biofuels properties on aircraft engine performance. *Aircr. Eng. Aerosp. Technol.* **2015**, *87*, 437–442. [CrossRef]
25. Liem, R.P.; Martins, J.R.; Kenway, G.K. Expected drag minimization for aerodynamic design optimization based on aircraft operational data. *Aerosp. Sci. Technol.* **2017**, *63*, 344–362. [CrossRef]
26. Zhu, J.H.; Zhang, W.H.; Xia, L. Topology optimization in aircraft and aerospace structures design. *Arch. Comput. Methods Eng.* **2015**, *23*, 595–622. [CrossRef]
27. Lei, R.; Bai, J.; Xu, D. Aerodynamic optimization of civil aircraft with wing-mounted engine jet based on adjoint method. *Aerosp. Sci. Technol.* **2019**, *93*, 105285. [CrossRef]
28. Gu, X.; Ciampa, P.D.; Jepsen, J.; Nagel, B. High fidelity aerodynamic optimization in distributed overall aircraft design. In Proceedings of the AIAA Aviation Forum, 17th AIAA/ISSMO Multidisciplinary Analysis and Optimization Conference, Washington, DC, USA, 13–17 June 2016. [CrossRef]
29. Lange, R.H. Review of unconventional aircraft design concepts. *J. Aircr.* **1988**, *25*, 385–392. [CrossRef]
30. Schmitt, D. Challenges for unconventional transport aircraft configurations. *Air Space Eur.* **2001**, *3*, 67–72. [CrossRef]

31. Iwanizki, M.; Wöhler, S.; Fröhler, B.; Zill, T.; Méheut, M.; Defoort, S.; Carini, M.; Gauvrit-Ledogar, J.; Liaboeuf, R.; Tremolet, A.; et al. Conceptual Design Studies of Unconventional Configurations. 3AF Aerospace Europe Conference 2020, Bordeaux. 2020. Available online: https://hal.archives-ouvertes.fr/hal-02907205 (accessed on 18 July 2021).
32. Bijewitz, J.; Seitz, A.; Isikveren, A.T.; Hornung, M. Multi-disciplinary design investigation of propulsive fuselage aircraft concepts. *Aircr. Eng. Aerosp. Technol.* **2016**, *88*, 257–267. [CrossRef]
33. Defoort, S.; Méheut, M.; Paluch, B.; Liaboeuf, R.; Murray, R.; Mincu, D.C.; David, J.M. Conceptual design of disruptive aircraft configurations based on High-Fidelity OAD process. In Proceedings of the AIAA Aviation Forum, 2018 Aviation Technology, Integration, and Operations Conference, Atlanta, GA, USA, 25–29 June 2018. [CrossRef]
34. Werner-Westphal, C.; Heinze, W.; Horst, P. Multidisciplinary integrated preliminary design applied to unconventional aircraft configurations. *J. Aircr.* **2008**, *45*, 581–590. [CrossRef]
35. Liebeck, R.H. Design of the blended wing body subsonic transport. *J. Aircr.* **2004**, *41*, 10–25. [CrossRef]
36. Qin, N.; Vavalle, A.; Le Moigne, A.; Laban, M.; Hackett, K.; Weinerfelt, P. Aerodynamic considerations of blended wing body aircraft. *Prog. Aerosp. Sci.* **2004**, *40*, 21–343. [CrossRef]
37. Okonkwo, P.; Smith, H. Review of evolving trends in blended wing body aircraft design. *Prog. Aerosp. Sci.* **2016**, *82*, 1–23. [CrossRef]
38. Cavallaro, R.; Demasi, L. Challenges, ideas, and innovations of joined-wing configurations: A concept from the past, an opportunity for the future. *Prog. Aerosp. Sci.* **2016**, *87*, 1–93. [CrossRef]
39. Wolkovitch, J. The joined wing: An overview. *J. Aircr.* **1986**, *23*, 161–178. [CrossRef]
40. Frediani, A.; Cipolla, V.; Rizzo, E. The Prandtl plane configuration: Overview on possible applications to civil aviation. In *Variational Analysis and Aerospace Engineering: Mathematical Challenges for Aerospace Design*; Springer Optimization and Its Applications; Springer: Boston, MA, USA, 2012; Volume 66. [CrossRef]
41. Frediani, A.; Rizzo, E.; Bottoni, C.; Scanu, J.; Iezzi, G. A 250 Passenger Prandtl plane transport aircraft preliminary design. *Aerotecnica Missili Spazio* **2005**, *84*. Available online: http://hdl.handle.net/11568/99885 (accessed on 18 July 2021).
42. Frediani, A. The Prandtl Wing. VKI, Lecture Series: Innovative Configurations and Advanced Concepts for Future Civil Transport Aircraft. 2005. Available online: https://perma.cc/XU6F-8YLG (accessed on 18 July 2021).
43. Frediani, A.; Cipolla, V.; Oliviero, F. Design of a prototype of light amphibious Prandtl Plane. In Proceedings of the AIAA SciTech Forum, 56th AIAA/ASCE/AHS/ASC Structures, Structural Dynamics, and Materials Conference, Kissimmee, FL, USA, 5−9 January 2015. [CrossRef]
44. Prandtl, L.; Induced Drag of Multiplanes. NACA TN-182. 1924. Available online: https://ntrs.nasa.gov/citations/19930080964 (accessed on 18 July 2021).
45. Frediani, A.; Montanari, G. Best wing system: An exact solution of the Prandtl's problem. In *Variational Analysis and Aerospace Engineering*; Springer Optimization and Its Applications; Springer: New York, NY, USA, 2009; Volume 33. [CrossRef]
46. Demasi, L.; Dipace, A.; Monegato, G.; Cavallaro, R. Invariant formulation for the minimum induced drag conditions of nonplanar wing systems. *AIAA J.* **2014**, *52*. [CrossRef]
47. PARSIFAL Project. Available online: https://perma.cc/5ULW-HCP4 (accessed on 18 July 2021).
48. Abu Salem, K.; Binante, V.; Cipolla, V.; Maganzi, M. PARSIFAL project: A breakthrough innovation in air transport. *Aerotecnica Missili Spazio* **2018**, *97*. [CrossRef]
49. Abu Salem, K. Studio Sulla Configurazione Aerodinamica di Velivoli Civili di Tipo PrandtlPlane di Piccole e Medie Dimensioni. M.Sc. Thesis, University of Pisa, Italy, 2016. Available online: https://etd.adm.unipi.it/theses/available/etd-06222016-110207/ (accessed on 18 July 2021).
50. Bishop, K. Assessment of the Ability of Existing Airport Gate Infrastructure to Accommodate Transport Category Aircraft with Increased Wingspan for Improved Fuel Efficiency. M.Sc. Thesis, Dept. of Aeronautics and Astronautics, Massachusetts Institute of Technology, Boston, MA, USA, 2012. Available online: http://hdl.handle.net/1721.1/76095 (accessed on 18 July 2021).
51. European Commission. Mobility for Growth—Breakthrough Innovation. Funding Action for Research and Innovation. 2015. Available online: https://ec.europa.eu/inea/en/news-events/newsroom/new-transport-projects-selected-horizon-2020-funding (accessed on 18 July 2021).
52. McMasters, J.; Paisley, D.; Hubert, R.; Kroo, I.; Bofah, K.; Sullivan, J.; Drela, M. Advanced configurations for very large subsonic Transport Airplanes. NASA CR 198351. 1996. Available online: https://ntrs.nasa.gov/citations/19970003675 (accessed on 18 July 2021).
53. Raymer, D.P. *Aircraft Design: A Conceptual Approach*; AIAA Education Series: Washington, DC, USA, 1992; ISBN 0-930403-51-7.
54. Association of European Airlines. *Short-Medium Range Aircraft AEA Requirements. Report G(T)*; AEA: Bonn, Germany, 1989.
55. Casarosa, C. *Meccanica del Volo*; Pisa University Press: Pisa, Italy, 2013; ISBN 978-8867410163.
56. Rizzo, E. Optimization Methods Applied to the Preliminary Design of Innovative Non Conventional Aircraft Configurations. Ph.D. Thesis, University of Pisa, Pisa, Italy, 2009. Available online: https://etd.adm.unipi.it/t/etd-05122010-103814/ (accessed on 18 July 2021).
57. Cappelli, L.; Costa, G.; Cipolla, V.; Frediani, A.; Oliviero, F.; Rizzo, E. Aerodynamic optimization of a large PrandtlPlane configuration. *Aerotecnica Missili Spazio* **2016**, *95*, 163–175. [CrossRef]
58. Abu Salem, K.; Palaia, G.; Cipolla, V.; Binante, V.; Zanetti, D.; Chiarelli, M. Tools and methodologies for box-wing aircraft conceptual aerodynamic design and aeromechanic analysis. *Mech. Ind.* **2021**, *22*, 1–19. [CrossRef]

59. Rizzo, E.; Frediani, A. Application of optimisation algorithms to aircraft aerodynamics. In *Variational Analysis and Aerospace Engineering*; Springer Optimization and Its Applications: New York, NY, USA, 2009. [CrossRef]
60. Addis, B.; Locatelli, M.; Schoen, F. Local optima smoothing for global optimization. *Optim. Methods Softw.* **2005**, *20*, 417–437. [CrossRef]
61. Drela, M.; Youngren, H. XFOIL 6.9 User Primer. Online Software Manual. 2001. Available online: https://perma.cc/7AGE-C3XU (accessed on 18 July 2021).
62. Drela, M.; Youngren, H. AVL 3.36 User Primer. Online Software Manual. 2017. Available online: https://perma.cc/R35R-W29F (accessed on 18 July 2021).
63. Beltramo, M.; Trapp, D.; Kimoto, B.; Marsh, D. Parametric Study of Transport Aircraft Systems Cost and Weight. Report NASA CR151970. 1977. Available online: https://ntrs.nasa.gov/citations/19770019162 (accessed on 18 July 2021).
64. Wells, D.; Horvath, B.; McCullers, L. The Flight Optimization System Weights Estimation Method. NASA/TM–2017–219627, Volume I; 2017. Available online: https://ntrs.nasa.gov/citations/20170005851 (accessed on 18 July 2021).
65. Frediani, A.; Cipolla, V.; Abu Salem, K.; Binante, V.; Picchi Scardaoni, M. Conceptual design of PrandtlPlane civil transport aircraft. *Inst. Mech. Eng. Part G J. Aerosp. Eng.* **2019**, *234*, 1675–1687. [CrossRef]
66. Mason, W.H. Analytic models for technology integration in aircraft design. *AIAA Aircr. Des. Syst. Op. Conf. Dayton* **1990**, *90*, 3262-CP. [CrossRef]
67. Cipolla, V.; Frediani, A.; Abu Salem, K.; Binante, V.; Rizzo, E.; Maganzi, M. Preliminary transonic CFD analyses of a PrandtlPlane transport aircraft. *Transp. Res. Procedia* **2018**, *29*, 82–91. [CrossRef]
68. ANSYS, Ansys Fluent—Fluid Simulation Software. Available online: https://perma.cc/L56W-V8FZ (accessed on 18 July 2021).
69. Fazalzadeh, S.; Scholz, D.; Mazidi, A.; Friswell, M. Flutter characteristics of typical wing sections of a box wing aircraft configuration. In Proceedings of the 3AF AEGATS Proceedings 2018, Toulouse, France, 23−25 October 2018. [CrossRef]
70. Divoux, N.; Frediani, A. The lifting system of a PrandtlPlane, Part 2: Preliminary study on flutter characteristics. In *Variational Analysis and Aerospace Engineering*; Springer Optimization and Its Applications: Boston, MA, USA, 2012. [CrossRef]
71. Cavallaro, R.; Bombardieri, R.; Silvani, S.; Demasi, L.; Bernardini, G. Aeroelasticity of the PrandtlPlane: Body freedom flutter, freeplay, and limit cycle oscillation. In *Variational Analysis and Aerospace Engineering: Mathematical Challenges for the Aerospace of the Future*; Springer Optimization and Its Applications: New York, NY, USA, 2016. [CrossRef]
72. Bombardieri, R.; Cavallaro, R.; Demasi, L. A historical perspective on the aeroelasticity of box Wings and PrandtlPlane with new findings. In Proceedings of the AIAA SciTech Forum, 57th AIAA/ASCE/AHS/ASC Structures, Structural Dynamics, and Materials Conference, San Diego, CA, USA, 4−8 January 2016. [CrossRef]
73. PARSIFAL Project Consortium. Aeroelastic Analysis of the Baseline PrandtlPlane. PARSIFAL Project Deliverables, D5.2. 2020. Available online: https://perma.cc/JYL5-K9ST (accessed on 18 July 2021).
74. Abu Salem, K. Development of Design Tools and Methods for Box-Wing Airplanes and Application of the PrandtlPlane Concept to a Short-Medium Range Aircraft. Ph.D. Thesis, University of Pisa, Pisa, Italy, 2021. Available online: https://etd.adm.unipi.it/ (accessed on 18 July 2021).
75. Picchi Scardaoni, M.; Binante, V.; Cipolla, V. WAGNER: A new code for parametrical structural study of fuselages of civil transport aircraft. *Aerotecnica Missili Spazio* **2017**, *96*, 136–147. [CrossRef]
76. 3DS Dassault Systems Simulia, ABAQUS Unified FEA. Available online: https://perma.cc/X8L3-JGSV (accessed on 18 July 2021).
77. Fuchte, J. Enhancement of Aircraft Cabin Design Guidelines with Special Consideration of Aircraft Turnaround and Short Range Operations. Ph.D. Dissertation, DLR-Forschungsbericht, Hamburg, Germany, 2014. Available online: https://perma.cc/YT3N-99VV (accessed on 18 July 2021).
78. Fuchte, J.; Nagel, B.; Gollnick, V. Weight and fuel saving potential through changed cabin and fuselage design. In Proceedings of the AIAA Aviation Forum, Aviation Technology, Integration, and Operations Conference, Los Angeles, California, USA, 12−14 August 2013. [CrossRef]
79. PARSIFAL Project Consortium. Structural Analysis of the Baseline PrandtlPlane. PARSIFAL Project Deliverables, D5.1. 2020. Available online: https://perma.cc/JYL5-K9ST (accessed on 18 July 2021).
80. Picchi Scardaoni, M.; Montemurro, M.; Panettieri, E. PrandtlPlane wing-box least-weight design: A multi-scale optimisation approach. *Aerosp. Sci. Technol.* **2020**, *106*, 106156. [CrossRef]
81. Cipolla, V.; Abu Salem, K.; Palaia, G.; Binante, V.; Zanetti, D. A DoE-based approach for the implementation of structural surrogate models in the early stage design of box-wing aircraft. *Aerosp. Sci. Technol.* **2021**, *117*, 106968. [CrossRef]
82. Torenbeek, E. Development and Application of a Comprehensive, Design-Sensitive Weight Prediction Method for Wing Structures of Transport Category Aircraft. Delft University of Technology, Faculty of Aerospace Engineering, Report LR-693. 1992. Available online: http://resolver.tudelft.nl/uuid:b45a61fe-317a-4201-82f0-dfae51ceb687 (accessed on 18 July 2021).
83. Filippone, A. *Advanced Aircraft Flight Performance*; Cambridge University Press: Cambridge, United Kingdom, 2012. [CrossRef]
84. Khadilkar, H.; Balakrishnan, H. Estimation of aircraft taxi fuel burn using flight data recorder archives. *Transp. Res. Part D* **2012**, *17*, 532–537. [CrossRef]
85. Abu Salem, K.; Palaia, G.; Bianchi, M.; Zanetti, D.; Cipolla, V.; Binante, V. Preliminary take-off analysis and simulation of PrandtlPlane commercial aircraft. *Aerotecnica Missili Spazio* **2020**, *99*, 203–216. [CrossRef]
86. Airbus. *Getting to Grips with Aircraft Performance*; Airbus SAS: Leiden, The Netherlands, 2002. Available online: https://perma.cc/FQ9P-FET4 (accessed on 18 July 2021).

87. Cipolla, V.; Frediani, A.; Abu Salem, K.; Picchi Scardaoni, M.; Nuti, A.; Binante, V. Conceptual design of a box-wing aircraft for the air transport of the future. In Proceedings of the AIAA Aviation Forum, 2018 Aviation Technology, Integration, and Operations Conference, Atlanta, GA, USA, 25−29 June 2018. [CrossRef]
88. Cipolla, V.; Abu Salem, K.; Picchi Scardaoni, M.; Binante, V. Preliminary design and performance analysis of a box-wing transport aircraft. In Proceedings of the AIAA SciTech 2020 Forum, Orlando, FL, USA, 6−10 January 2020. [CrossRef]
89. Carini, M.; Méheut, M.; Kanellopoulos, S.; Cipolla, V.; Abu Salem, K. Aerodynamic analysis and optimization of a boxwing architecture for commercial airplanes. In Proceedings of the AIAA SciTech 2020 Forum, Orlando, FL, USA, 6−10 January 2020. [CrossRef]
90. PARSIFAL Project Consortium. Requirements for the Adoption of the PrandtlPlane as a Mean of Transport. PARSIFAL Project Deliverables, D 2.1. 2017. Available online: https://perma.cc/BD3L-895C (accessed on 18 July 2021). (public).
91. International Civil Aviation Organization. *Aerodromes: Volume I—Aerodrome Design and Operations. International Standards and Recommended Practices*; ICAO Annex 14: Montréal, QC, Canada, 2009.
92. CeRAS—Central Reference Aircraft System. Available online: https://ceras.ilr.rwth-aachen.de/ (accessed on 18 July 2021).
93. Risse, K.; Schäfer, K.; Schültke, F.; Stumpf, E. Central reference aircraft data system (CeRAS) for research community. *CEAS Aeronaut. J.* **2016**, *7*, 121–133. [CrossRef]
94. Airbus, Aircraft characteristics—Airport and Maintenance Planning, Airbus SAS. 2014. Available online: https://perma.cc/XM64-GZMT (accessed on 18 July 2021).
95. Picchi Scardaoni, M.; Frediani, A. General closed-form solution of piecewise circular frames of aircraft. *AIAA J.* **2019**, *57*, 1338–1342. [CrossRef]
96. Bottoni, C.; Scanu, J. Preliminary Design of a 250 Passenger PrandtlPlane Aircraft. M.Sc. Thesis, University of Pisa, Pisa, Italy, 2004. Available online: https://etd.adm.unipi.it/theses/available/etd-09072004-140314/ (accessed on 18 July 2021).
97. Schiktanz, D.; Scholz, D. Box wing fundamentals—An aircraft design perspective. In Proceedings of the DGLR: Deutscher Luft und Raumfahrtkongress 2011, Bremen, Germany, 27–29 September 2011; pp. 601–615, ISBN 978-3-932182-74-X. Document ID: 241353. Available online: https://perma.cc/2Q7R-WFAF (accessed on 18 July 2021).
98. Picchi Scardaoni, M.; Magnacca, F.; Massai, A.; Cipolla, V. Aircraft turnaround time estimation in early design phases: Simulation tools development and application to the case of box-wing architecture. *J. Air Transp. Manag.* **2021**, *96*, 102122. [CrossRef]
99. PARSIFAL Project Consortium. Report on Operational and Economic Assessment. PARSIFAL Project Deliverables, D 1.2. 2020. Available online: https://perma.cc/U3QF-JQL7 (accessed on 18 July 2021). (public).
100. Cipolla, V.; Abu Salem, K.; Bachi, F. Preliminary stability analysis methods for PrandtlPlane aircraft in subsonic conditions. *Aircr. Eng. Aerosp. Technol.* **2018**, *91*, 525–537. [CrossRef]
101. Cipolla, V.; Abu Salem, K.; Palaia, G.; Binante, V.; Zanetti, D. A semi-empirical VLM-based method for the prediction of maximum lift coefficient of box-wing aircraft. *J. Aerosp. Eng.* **2021**, under review.
102. Arkell, D. Moving toward the Middle, Frontiers Magazine: Boeing. 2003. Available online: https://perma.cc/EK8C-B7RP (accessed on 18 July 2021).
103. Tasca, A.L.; Cipolla, V.; Abu Salem, K.; Puccini, M. Innovative box-wing aircraft: Emissions and climate change. *Sustainability* **2021**, *13*, 3282. [CrossRef]